IA|BE PROSPECTIVE MORTALITY TABLES 2020

NOVEMBER 2020

The IA|BE 2020 mortality projection for the Belgian population

Katrien Antonio [*1,2], Sander Devriendt [†] , and Jens Robben [‡]

[1]Faculty of Economics and Business, KU Leuven, Belgium.
[2]Faculty of Economics and Business, University of Amsterdam, The Netherlands.

February 24, 2021

1 Introduction

Stochastic mortality projection models are a useful tool in the quantification of the evolution of mortality rates over time and the measurement and management of longevity risk, as Barrieu et al. (2012) indicate. In this paper we put focus on the development of a fully stochastic mortality projection model for annual data collected for the Belgian population. While this is the most relevant perspective when valuing life contingent risks, mortality data can also be monitored and analysed at a more granular level, see e.g. the weekly data monitored for Belgium by Sciensano in the Belgian Mortality Modelling (Be-MOMO) project (Cox et al., 2010) and the EuroMOMO project at European level.[1]

The development of mortality forecasting models has received wide coverage in the actuarial, demographic and statistical literature, starting from the seminal work by Lee & Carter ([LC]) (Lee and Carter (1992)). Antonio et al. (2015) present a follow-up on the 2002 mortality study of the former KVBA-ARAB (now: Institute of Actuaries in Belgium [IA|BE]) (see Lambrechts (2001), Brouhns et al. (2002a), Delfosse and Boelen (2002)). Building upon the work of Koninklijk Actuarieel Genootschap (2014) ([KAG]), the IA|BE 2015 mortality projection model is a fully stochastic projection model of Li & Lee ([LL]) type, see Li and Lee (2005). Hence, it is a multi-population model that projects Belgian mortality rates using Belgian mortality data together with observed mortality statistics gathered on a collection of European countries with a similar standard of living. For each gender, a Lee & Carter model is imposed for the European mortality trend as well as for the Belgian deviation from this common trend. By combining mortality data from different, but comparable countries a more robust model with more stable trends is constructed.

Antonio et al. (2017) provides an in-depth discussion of the multi-population mortality projection models produced by the professional actuarial associations in Belgium and the Netherlands.

[*]Corresponding author. E-mail address: katrien.antonio@kuleuven.be
[†]Voluntary research assistant on the mortality project at KU Leuven, AFI Department, Insurance Research Group. This paper reflects the personal views of the author and not the views of his employer.
[‡]Research assistant on the mortality project at KU Leuven, AFI Department, Insurance Research Group.
[1]See https://epistat.wiv-isp.be/momo/ for information about the Be-MOMO project.

Next to a discussion of the technical foundations and model choices, the 2017 paper also sketches four possible applications of the model: the calculation and projection of life expectancies (period and cohort) to enhance insight in their future evolution, the calculation of actuarial pension corrections as suggested by the Belgian Commissie Pensioenhervorming 2020-2040, the computations behind the Dutch legal retirement age updating mechanism, as well as an illustration of the reserve calculations for a typical portfolio with pension liabilities.

Frequent updates of mortality projection models are key. These include the collection of new data points as they unfold over time, the re-calibration of the model parameters, and - if necessary - the incorporation of methodological changes to construct resilient forecasting models. In that respect, KAG (2016, 2018) incorporates the correlation between the mortality trends of both men and women. In the KAG (2020) report, two extra modifications have been made compared to KAG (2018). First, an intercept is added to the time series model for the Dutch deviation from the European mortality trend, for both males and females. Second, the calibration of the Dutch deviation no longer uses data from 1970 but from 1983 on. However, Dutch data from 1970 is still used for the calibration of the European mortality trend.

Our report presents an update of the forecasting methodology used in Antonio et al. (2015) and Antonio et al. (2017). In line with KAG (2016, 2018) we model male and female mortality data jointly, within the multi-population Li and Lee model proposed for Belgium in Antonio et al. (2015). In addition, we include an intercept in the time series to model the Belgian period effect for males and females, in line with KAG (2020). Moreover, we investigate the effect of a higher lag-order in the autoregressive time series process to model the Belgian period effect. We do this to attain a long-term convergence between the Belgian mortality trend and the European mortality trend and to investigate the sensitivity of the projection with respect to different time series models. On top of that, we asses the uncertainty of some parameter estimates in the calibrated model and in the time series dynamics by means of Poisson bootstrapping.

The necessity of frequent updates of mortality projection models is more relevant than ever in light of the ongoing covid-19 pandemic. Our contribution includes annual data collected for the Belgian population up to (and including) the year 2019. With a pandemic that reached Belgium in 2020 and is still ongoing at the time of writing, it is difficult to assess the potential impact of covid-19 on our forecasts. By creating virtual data points for 2020, incorporating the deaths as observed until mid 2020, we assess this potential impact by recalibrating the proposed model on the data enriched with the virtual data points. This impact assessment is covered in a separate note.

This report is organized as follows. A technical description of the model and a discussion of methodological changes compared to the 2015 mortality projection is provided in Section 2. The use of the model and its applications are documented in Section 3. Section 4 quantifies the impact on the cohort life expectancy in 2020, when making the step from the IA|2015 to the IA|2020 model in terms of new data and methodological updates. Section 5 concludes. Tables with parameter estimates and the resulting IA|BE 2020 mortality projection for Belgium are available in an online appendix. Further, Appendix A documents the data sources used in this paper, Appendix B motivates the choice of the calibration period, Appendix C deals with high-order autoregressive time series processes and Appendix D discusses parameter uncertainty.

2 Technical description of the model

2.1 Notation

Let $\mathcal{X}$ denote a collection of ages and $\mathcal{T}$ a collection of years. We denote with $q_{x,t}$, for $x \in \mathcal{X}$ and $t \in \mathcal{T}$, the probability that a person who is alive at 1 January of year t, and who was born on 1 January of year $t-x$, will be death on 1 January of year $t+1$. We call $q_{x,t}$ the mortality rate at exact age x in year t. Stochastic mortality projection models either directly model (a transformation of) $q_{x,t}$ or they model the force of mortality, $\mu_{x,t}$. Under the assumption of piecewise constant force of mortality, i.e. $\mu_{x+s,t+s} = \mu_{x,t}$ for $0 \leqslant s < 1$, the following relation holds between $q_{x,t}$ and $\mu_{x,t}$:

$$q_{x,t} \quad = \quad 1 - \exp\left(-\mu_{x,t}\right). \tag{1}$$

Expression (1) enables switching from the force of mortality to the mortality rate, and vice versa, in a straightforward way. For more details about these concepts and additional reading material we refer to Pitacco et al. (2009).

All the aforementioned quantities are referred to as being in 'exact age' or 'period age'. They apply to people who have exact age x at exact time t. As Cairns et al. (2016) indicate, one has to be wary of any data quality issues when receiving data from different sources or even from the same source at different times. For example, not all data sources work with the period or exact age definitions, but instead apply 'cohort' or 'completed years' definitions. A cohort refers to all people born in the same year. On 1 January of year t, a cohort born in year $t-x-1$ will have 'completed' the exact age x and not reached age $x+1$. As some institutions publish data on deaths and exposures only in the cohort representation while others use the exact age definitions, it will be necessary to establish a link between the cohort and period deaths and exposures. Such a link enables to transform data from one format to the other, and is documented in detail in Antonio et al. (2017). In this report we always use the period age definition unless explicitly stated differently.

2.2 Data

In our study, we calibrate mortality models by using annual data on the observed number of deaths, $d_{x,t}$, and the corresponding exposures to risk, $E_{x,t}$, for a set of countries over a specified calibration period and over a specified age range. We collect this data from three data sources. The main data source is the Human Mortality Database[2] ([HMD]). The second one is Eurostat[3] for the years for which there is no data (yet) available in the HMD. We use the third data scource, Statistics Belgium ([Statbel])[4], to acquire the most recent mortality data for Belgium.

Further, we use a collection of 14 European countries, namely Belgium, The Netherlands, Luxembourg, Norway, Switzerland, Austria, Ireland, Sweden, Denmark, Germany, Finland, Iceland, United Kingdom and France. The selected countries are the ones with a Gross Domestic

[2] This database is available at www.mortality.org.

[3] Eurostat is the statistical office of the European Union, https://ec.europa.eu/eurostat. We download the considered data sets at https://ec.europa.eu/eurostat/data/database.

[4] "Statbel, the Belgian statistical office, collects, produces and disseminates reliable and relevant figures on the Belgian economy, society and territory." (https://statbel.fgov.be/en)

Product ([GDP]) per capita above the European average.[5] In line with Koninklijk Actuarieel Genootschap (2016, 2018, 2020) the collection of countries used in this report differs from the set considered in Antonio et al. (2015) in two ways:

1. from 1970 on, we extend England & Wales with Northern-Ireland and Scotland to obtain data from the United Kingdom as a whole. This facilitates collecting the necessary data.

2. in addition, from 1990 on, we add data from East Germany due to the German unification. Hence, before 1990, we only use data from West Germany. From 1990 on, we work with data collected for Germany as a whole.

We collect the data for age range $\{0, \ldots, 90\}$ and historical period $\{1970, \ldots, 2018\}$. Later on, we will extrapolate the calibrated and projected mortality rates towards higher ages using the method of Kannistö (Kannisto, 1994). From the HMD database we use the tables 'Deaths' and 'Exposure to risk' in 1×1 format. These files contain the number of deaths and exposures for the selected country per year, per sex and per age in period format. Eurostat only lists the period number of deaths.[6] However, we obtain the exposures in period format using databases on the population size[7] at 1 January of each year t, say $P_{x,t}$, and the cohort number of deaths[8], say $C_{x,t}$, as defined according to the protocol of HMD.[9] The cohort number of deaths $C_{x,t}$ refers to the number of people who were born in year $t-x-1$ and died in year t. Adjusting to the HMD protocol requires the following transformations:

$$\begin{aligned} E_{x,t} &= \frac{1}{2}\left(P_{x,t} + P_{x,t+1}\right) + \frac{1}{6}\left(\frac{1}{2}C_{x,t} - \frac{1}{2}C_{x+1,t}\right) \quad \text{if } x > 0 \\ E_{0,t} &= \frac{1}{2}\left(P_{0,t} + P_{0,t+1}\right) + \frac{1}{6}\left(C_{0,t} - \frac{1}{2}C_{1,t}\right). \end{aligned}$$

At Statbel, deaths are available in period and cohort format.[10] Population sizes at 1 January of each year t can be consulted as well on Statbel.[11] In line with the transformations applied to the data collected from Eurostat, we deduce the period exposures from the Statbel data by following the above explained HMD protocol.

We proceed with a data set of deaths and exposures in period format for a collection of 13 European countries during the period 1970-2018 and for Belgium during 1970-2019. We extract these data for males and females. For reproducibility reasons, Appendix A lists the date of the last modification of each of the data sets used in this report.

[5] Source: World Bank Data for 2018 on GDP per capita in US dollar, https://data.worldbank.org/indicator/NY.GDP.PCAP.CD. The GDP per capita for the Euro area is 39,927.6 USD in 2018 and the fourteen countries listed are the countries in Europe with a higher GDP per capita.

[6] This information is available at https://appsso.eurostat.ec.europa.eu/nui/show.do?dataset=demo_magec&lang=en.

[7] This database can be consulted at https://appsso.eurostat.ec.europa.eu/nui/show.do?dataset=demo_pjan&lang=en.

[8] This database can be found at https://appsso.eurostat.ec.europa.eu/nui/show.do?dataset=demo_mager&lang=en.

[9] This protocol is available from https://www.mortality.org/Public/Docs/MethodsProtocol.pdf.

[10] These databases can be downloaded from https://statbel.fgov.be/nl/themas/bevolking/sterfte-en-levensverwachting/sterftetafels-en-levensverwachting#figures

[11] See https://bestat.statbel.fgov.be/bestat/crosstable.xhtml?view=5fee32f5-29b0-40df-9fb9-af43d1ac9032.

We visualize the composition of the data set in terms of deaths and exposures in Figure 1. Figure 2 visualizes the evolution of the period life expectancies at birth for the 14 European countries in the data set, downloaded from the HMD. We observe a more stable pattern in the evolution of the life expectancies from 1970 on, motivating the start year of the data collection.

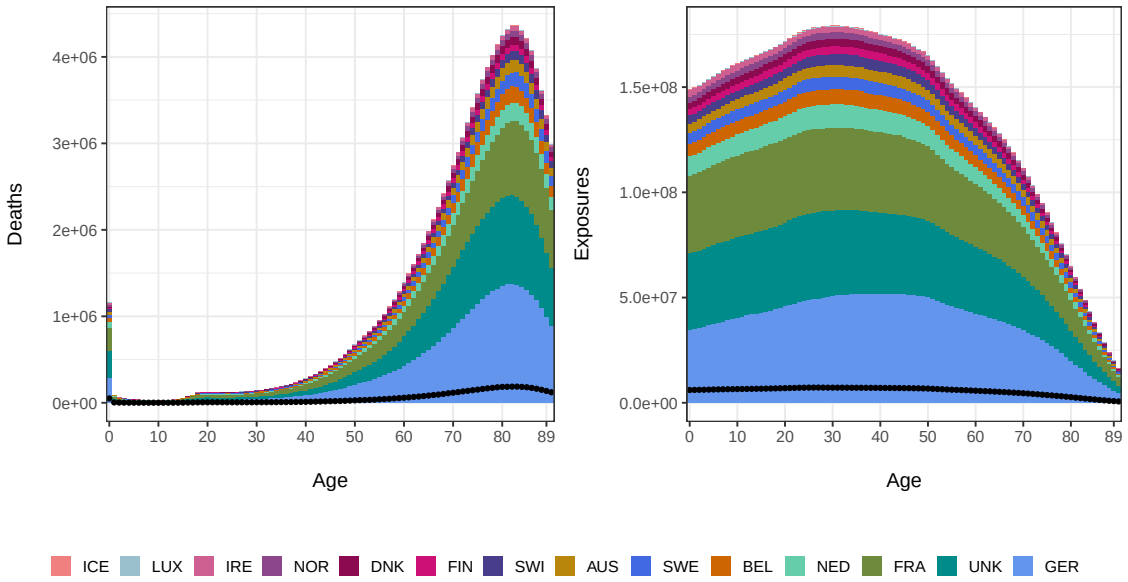

Figure 1: The combined male and female exposures (left panel) and deaths (right panel) that are stacked per country for all ages during the period 1970-2019 (Belgium) or 1970-2018 (other European countries). The country with the largest exposure and deaths in the data set is at the bottom of the graph. The black points indicate the combined male and female deaths and exposures for Belgium.

2.3 Model specification

The mortality model structures the logarithm of the force of mortality for Belgium, $\mu_{x,t}^{\text{BEL}}$, as follows

$$\ln \mu_{x,t}^{\text{BEL}} = \ln \mu_{x,t}^{\text{EU}} + \ln \tilde{\mu}_{x,t}^{\text{BEL}} \tag{2}$$

$$\ln \mu_{x,t}^{\text{EU}} = A_x + B_x K_t \tag{3}$$

$$\ln \tilde{\mu}_{x,t}^{\text{BEL}} = \alpha_x + \beta_x \kappa_t. \tag{4}$$

We recognize two times a Lee & Carter specification; (3) is a LC model for the European evolution of mortality (driven by $\mu_{x,t}^{\text{EU}}$) and (4) is a LC model for the Belgian deviation from this common trend (specified by $\tilde{\mu}_{x,t}^{\text{BEL}}$). We calibrate this model on data with ages ranging from 0 up to 90, thus $\mathcal{X} = \{0, \ldots, 90\}$, and a calibration period from t_{start} up to 2018 for the European mortality trend, denoted with $\bar{\mathcal{T}} = \{t_{\text{start}}, \ldots, 2018\}$, and up to 2019 for the Belgian deviation from this European trend, say $\mathcal{T} = \{t_{\text{start}}, \ldots, 2019\}$. The calibration methodology is described in Section 2.4. For the time dependent parameters, K_t and κ_t, the following time series models

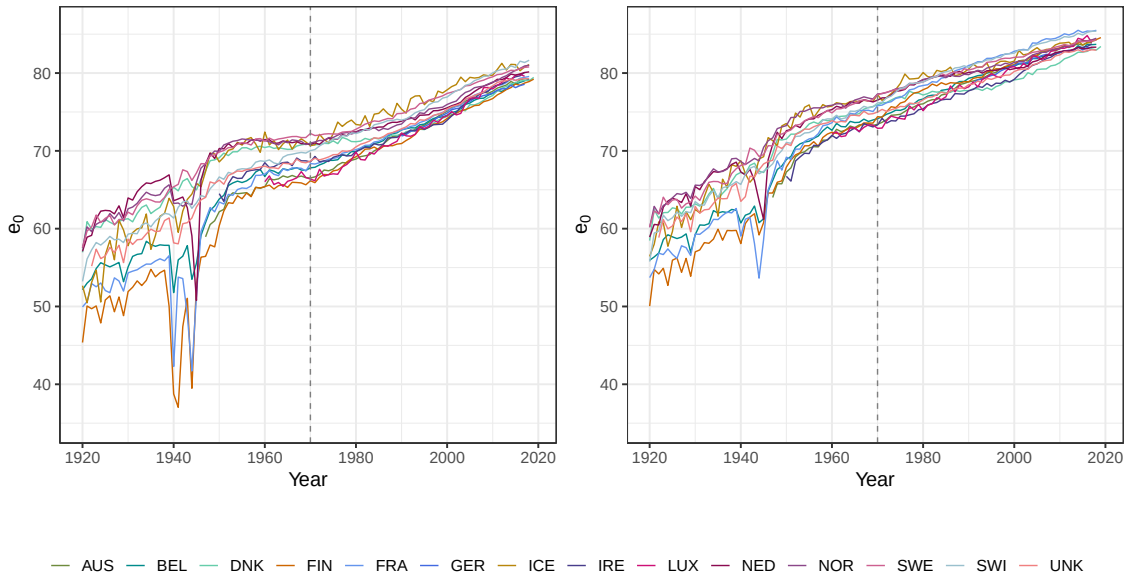

Figure 2: The evolution of the period life expectancies at birth for each of the 14 European countries in the data set for males (right panel) and females (left panel) in the period from 1920 on.

are used

$$K_{t+1} = K_t + \theta + \varepsilon_{t+1} \tag{5}$$
$$\kappa_{t+1} = c + \phi\kappa_t + \delta_{t+1}, \tag{6}$$

for males and females. This leads to four stochastic processes $(K_t^M, \kappa_t^M, K_t^F, \kappa_t^F)$. The dynamics of the common period effect (see (5)), K_t, are modelled with a Random Walk with Drift ([RWD]), where θ is the drift and ε_{t+1} is white noise. The Belgian period effect (see (6)) κ_t follows, in contrast with the Antonio et al. (2015) model, an AR(1) process with intercept c. With this methodological change the AR(1) parameter in the κ_t process no longer depends on the linear identifiability constraint we impose on κ_t, see the discussion in Section 2.4. Moreover, by including an intercept in the AR(1) process, the κ_t may converge to a non-zero value. This allows for an extra gap, besides the age effect α_x, between the long term projected mortality rates for Belgium and Europe.

Further, in contrast to Antonio et al. (2015), we jointly model the time series dynamics for men and women by assuming a multivariate Gaussian distribution with mean $(0, 0, 0, 0)$ and covariance matrix $\boldsymbol{C}$ for the error terms $\left(\varepsilon_t^M, \delta_t^M, \varepsilon_t^F, \delta_t^F\right)$. We calibrate the parameters in these time series specifications on the estimated K_t and κ_t parameters, for $t \in \mathcal{T}$, and use these dynamics to forecast $\mu_{x,t}^{\text{BEL}}$ for $t \in \{2020, 2021, \ldots, t_{\max}\}$. This projection strategy is documented in Section 2.5.

2.4 Calibration

We calibrate the parameters (A_x, B_x, K_t, α_x, β_x and κ_t) in the LL specification using Maximum Likelihood Estimation ([MLE]). Following the seminal paper by Brouhns et al. (2002b) we assume a Poisson distribution for the number of deaths random variable $D_{x,t}$, with mean $E_{x,t} \cdot \mu_{x,t}$ and $E_{x,t}$ the observed exposure to risk. To avoid identification problems in the LL model we use a

conditional maximum likelihood approach as in Li (2013). We calibrate the common parameters (i.e. A_x, B_x and K_t) in a first step, followed by the calibration of the Belgian parameters (i.e. α_x, β_x and κ_t) in a second step.

1. Observed deaths to calibrate the European trend, $d_{x,t}^{\text{EU}}$, and corresponding exposures to risk, $E_{x,t}^{\text{EU}}$, are obtained from the Human Mortality Database and Eurostat (see Section 2.2) by aggregating deaths and exposures over the 14 selected countries, using $\mathcal{X} = \{0, \ldots, 90\}$ and $\mathcal{T} = \{t_{\text{start}}, \ldots, 2018\}$. We maximize the following Poisson likelihood

$$\max_{A_x, B_x, K_t} \prod_{x \in \mathcal{X}} \prod_{t \in \mathcal{T}} (E_{x,t}^{\text{EU}} \mu_{x,t}^{\text{EU}})^{d_{x,t}^{\text{EU}}} \cdot \exp\left(-E_{x,t}^{\text{EU}} \mu_{x,t}^{\text{EU}}\right) / (d_{x,t}^{\text{EU}}!), \tag{7}$$

   with $\mu_{x,t}^{\text{EU}} = \exp\left(A_x + B_x K_t\right)$. We apply the Lee & Carter parameter constraints to identify parameters in a unique way, namely $\sum_{t \in \mathcal{T}} K_t = 0$ and $\sum_{x \in \mathcal{X}} B_x^2 = 1$.

2. We have data for Belgium up to 2019 and for the other 13 European countries up to 2018. We want to include the most recent data of Belgium to calibrate the mortality model. Therefore, we linearly extrapolate the parameter estimates K_t for the year 2019:

$$K_{2019} = K_{2018} + (K_{2018} - K_{t_{\text{start}}}) / (2018 - t_{\text{start}}).$$

   The linear extrapolation is justified by the linear pattern of the estimated K_t parameters, as can be seen in Figures 3 and 5.

3. We calibrate the parameters for Belgium (i.e. α_x, β_x and κ_t) by maximizing the following Poisson likelihood, conditional on the common parameters estimated in step 1 of this procedure. Thus,

$$\max_{\alpha_x, \beta_x, \kappa_t} \prod_{x \in \mathcal{X}} \prod_{t \in \mathcal{T}} (E_{x,t}^{\text{BEL}} \mu_{x,t}^{\text{BEL}})^{d_{x,t}^{\text{BEL}}} \cdot \exp\left(-E_{x,t}^{\text{BEL}} \mu_{x,t}^{\text{BEL}}\right) / (d_{x,t}^{\text{BEL}}!), \tag{8}$$

   where $\mu_{x,t}^{\text{BEL}} = \mu_{x,t}^{\text{EU}} \cdot \exp\left(\alpha_x + \beta_x \kappa_t\right)$. We calibrate the parameters for Belgium on ages $\mathcal{X} = \{0, \ldots, 90\}$ and years $t \in \mathcal{T} = \{t_{\text{start}}, \ldots, 2019\}$. Once again we normalize the estimated parameters by imposing $\sum_{t \in \mathcal{T}} \kappa_t = 0$ and $\sum_{x \in \mathcal{X}} \beta_x^2 = 1$.

We apply this calibration strategy[12] separately for males and females. We illustrate the resulting parameter estimates for male data in Figure 3 (European parameters) and Figure 4 (Belgian parameters). Figures 5 and 6 show the corresponding results for females. An online appendix coming with this report lists all parameter estimates.

2.5 Projection

Calibrating the time series models. The mortality model specified in Section 2.3 together with the time dynamics specified in (5) and (6) allows to generate future scenarios of mortality. First, we calibrate the time series models to the parameter estimates $\{(K_t, \kappa_t) \mid t \in \mathcal{T}\}$ with $\mathcal{T} = \{t_{\text{start}}, \ldots, 2019\}$ simultaneously for males and females. As explained in Section 2.3, we hereby assume a multivariate Gaussian distribution for the error terms $\left(\varepsilon_t^M, \delta_t^M, \varepsilon_t^F, \delta_t^F\right)$ with mean $(0, 0, 0, 0)$ and covariance matrix $\boldsymbol{C}$. The error terms are independent and identically distributed for all t. The parameters θ^M, θ^F, c^M, c^F, ϕ^M, ϕ^F and $\boldsymbol{C}$, used in the time series specifications, are estimated using maximum likelihood.[13]

[12] We use routines written in `R`.

[13] In `R` we use Seemingly Unrelated Regression through the package `systemfit`, we use the function `systemfit` with options `method="SUR"` and `methodResidCov="noDfCor"`.

Stability of the AR(1)-process. κ_t tends to the intercept c when t tends to infinity if the AR(1) process in Equation (6) is stable. That is: the parameter estimate $\hat{\phi}$ in this AR(1) process should be smaller than 1 in absolute value. Initial experiments with a calibration period starting from 1970 on illustrated that this stability is not always safeguarded. We propose in Appendix B and C two solutions for this issue:

1. adjust the calibration period by increasing the start year of the calibration period.
2. increase the lag of the autoregressive process in order to find a stationary and stable AR(k) process for the Belgian period effect κ_t.

Based on the findings in Appendix B and C we opt for the adjusted calibration strategy, leading to the same start year 1988 in calibration periods $\bar{\mathcal{T}}$ (European mortality trend) and $\mathcal{T}$ (Belgian deviation trend).

2.6 The resulting mortality projection model

We calibrate the proposed LL mortality model on the chosen calibration periods $\bar{\mathcal{T}} = \{1988, 1989, \ldots, 2018\}$ for the European mortality trend and $\mathcal{T} = \{1988, 1989, \ldots, 2019\}$ for the Belgian deviation of this trend. The choices are motivated by the findings in Appendix B and C. The estimated parameters $\hat{A}_x$, $\hat{B}_x$, $\hat{K}_t$, $\hat{\alpha}_x$, $\hat{\beta}_x$ and $\hat{\kappa}_t$ are shown in Figures 3, 4, 5 and 6 for both males and females. Table 1 lists the adjusted parameter estimates in the time series specifications for $\hat{K}_t^M$, $\hat{\kappa}_t^M$, $\hat{K}_t^F$ and $\hat{\kappa}_t^F$, including the estimated four-dimensional covariance matrix of the error terms $\hat{\boldsymbol{C}}$. As expected, the AR(1) parameter in the time series for the male and female Belgian period effect is now smaller than one. This leads to stable AR(1) processes for the time series of $\hat{\kappa}_t^M$ and $\hat{\kappa}_t^F$. Because of the inclusion of the long-term gap c and the age effect α_x in the Belgian deviation trend κ_t, we do allow for a potential gap between the European and Belgian mortality rates on a long-term basis.

	$\hat{\theta}^{(BEL)}$	$\hat{c}^{(BEL)}$	$\hat{\phi}^{(BEL)}$	$\hat{\boldsymbol{C}}^{(BEL)}$				
					ε_t^M	δ_t^M	ε_t^F	δ_t^F
Male	-0.2285	0.0140	0.9682	ε_t^M	0.0291	0.0014	0.0353	0.0058
				δ_t^M	0.0014	0.0249	-0.0016	-0.0096
Female	-0.1882	-0.0240	0.9226	ε_t^F	0.0353	-0.0016	0.0458	0.0089
				δ_t^F	0.0058	-0.0096	0.0089	0.0211

Table 1: Time series parameter estimates using European and Belgian data, male and female data, ages 0-90, years 1988-2019.

Figure 3: Estimated common parameters, male data, ages 0-90, years 1988-2019: $\hat{A}_x$, $\hat{B}_x$ and $\hat{K}_t$.

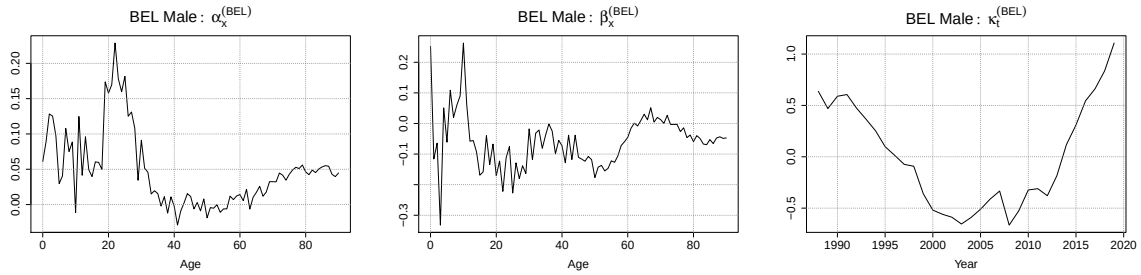

Figure 4: Estimated parameters for Belgium, male data, ages 0-90, years 1988-2019: $\hat{\alpha}_x$, $\hat{\beta}_x$ and $\hat{\kappa}_t$.

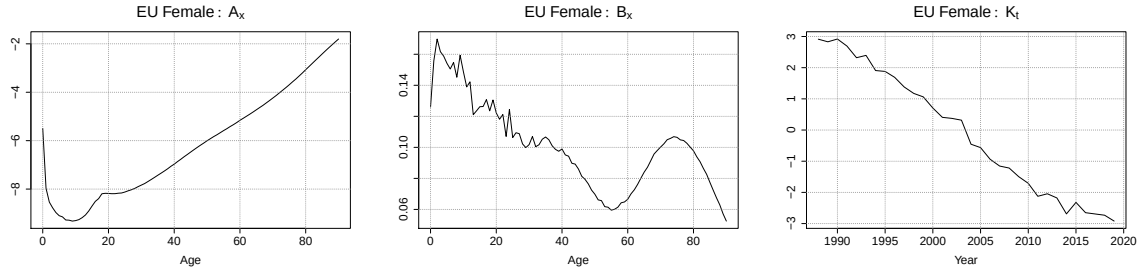

Figure 5: Estimated common parameters, female data, ages 0-90, years 1988-2019: $\hat{A}_x$, $\hat{B}_x$ and $\hat{K}_t$.

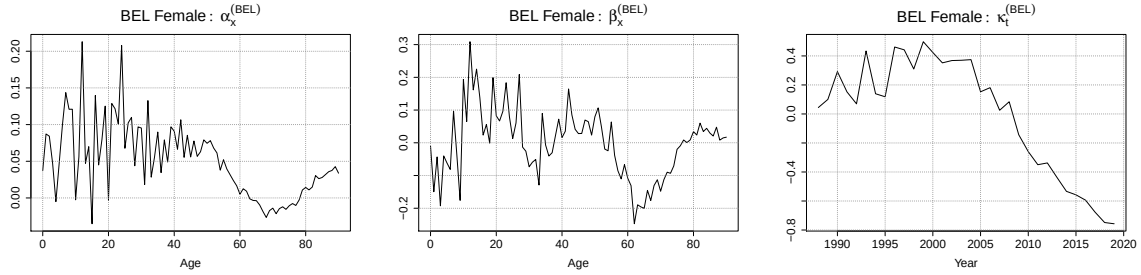

Figure 6: Estimated parameters for Belgium, female data, ages 0-90, years 1988-2019: $\hat{\alpha}_x$, $\hat{\beta}_x$ and $\hat{\kappa}_t$.

Goodness-of-fit Next, we examine the goodness-of-fit of our proposed mortality model by constructing a heatmap of the Pearson residuals for males and females. In the case of Poisson

regression, the Pearson residual for the observed death count $d_{x,t}^{\text{BEL}}$ is defined as:

$$\frac{d_{x,t}^{\text{BEL}} - E_{x,t}^{\text{BEL}} \hat{\mu}_{x,t}^{\text{BEL}}}{\sqrt{E_{x,t}^{\text{BEL}} \hat{\mu}_{x,t}^{\text{BEL}}}}.$$

Figure 7 displays the corresponding heatmaps. Overall the model captures the period and age effects very well. However, we observe one cohort-effect in the Pearson residuals, starting around the age of 70 in 1988. We decide not to include cohort effects in our mortality model for three reasons. First, the diagonal trends in these heatmaps are limited and, second, mortality models with cohort parameters are known to be less robust. Third, cohort parameters are more difficult to project with meaningful time series specifications (see the discussion in Antonio et al. (2017)).

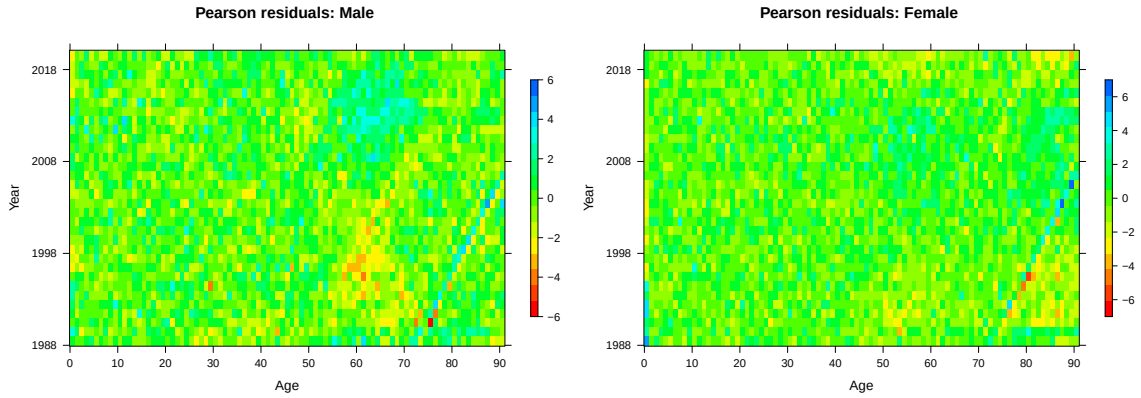

Figure 7: Heatmaps of the pearson residuals resulting from the constructed mortality model for males (left panel) and females (right panel): ages 0-90, years 1988-2019.

Generating future scenarios of mortality. Future mortality scenarios can be generated using the following step by step approach. For each future scenario $i = 1, \ldots, N$, and with t running from 2020 to some specific end year $t_{\max}$, we use the following strategy.

1. We simulate future $(K_t^{M,i}, \kappa_t^{M,i}, K_t^{F,i}, \kappa_t^{F,i})$ using the time dynamics specified in (5) and (6), with parameter estimates as listed in Table 1. We hereby start with $(\hat{K}_{2019}^M, \hat{\kappa}_{2019}^M, \hat{K}_{2019}^F, \hat{\kappa}_{2019}^F)$ as obtained with the calibration strategy from Section 2.4. These values are listed in the online appendix. We generate $(\varepsilon_t^M, \delta_t^M, \varepsilon_t^F, \delta_t^F)$ from a multivariate Gaussian distribution with mean $(0, 0, 0, 0)$ and covariance matrix $\hat{\boldsymbol{C}}$, as listed in Table 1.

2. Using the simulated $(K_t^{M,i}, \kappa_t^{M,i}, K_t^{F,i}, \kappa_t^{F,i})$ for $t = 2020, \ldots, t_{\max}$, we obtain $\mu_{x,t}^{\text{BEL},i}$ using (2), (3) and (4) and the age specific parameter estimates $(\hat{A}_x, \hat{\alpha}_x, \hat{B}_x, \hat{\beta}_x)$.

Figure 8 illustrates the projection of the time dependent parameters K_t and κ_t for males and females. We generate 10 000 scenarios and show the corresponding fan charts (formed by the median, 0.5% and 99.5% quantiles).

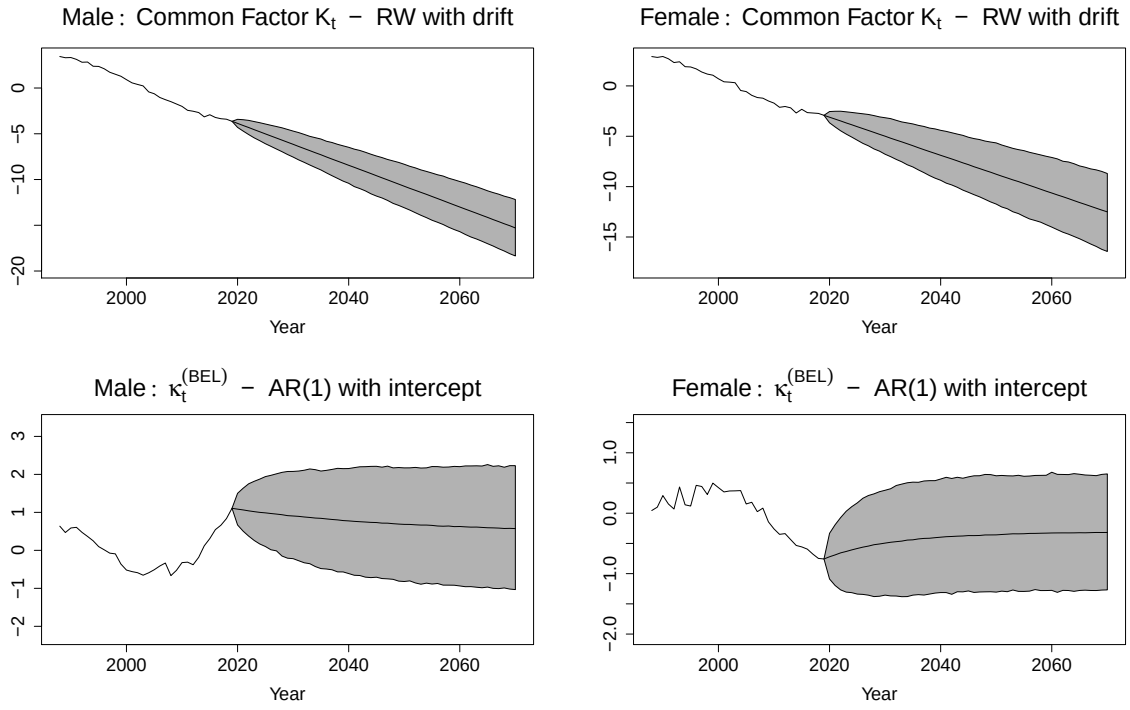

Figure 8: Projection of time dependent parameters: K_t and κ_t, male (left) and female (right) data, ages 0-90, years 1988-2070. We plot 0.5% quantile, median and 99.5% quantile obtained from 10 000 simulations.

Closing for old ages. We use Kannisto (1994) to close each mortality scenario for old ages, say $x \in \{91, 92, \ldots, 120\}$. This mortality law is chosen from a comparative analysis of techniques to close mortality tables, documented in Antonio (2012). This parametric law specifies the force of mortality in each scenario i, for ages $x > 90$ and a specific year t, as follows:

$$\mu^i_{x,t} \quad = \quad \frac{\phi_1^{i,t} \exp\left(\phi_2^{i,t} x\right)}{1 + \phi_1^{i,t} \exp\left(\phi_2^{i,t} x\right)}. \tag{9}$$

We estimate (ϕ^i_1, ϕ^i_2) for each scenario i and year t using the relation (see Doray (2008))

$$\text{logit } \mu^i_{x,t} \quad = \quad \log\left(\phi_1^{i,t}\right) + \phi_2^{i,t} x, \tag{10}$$

which we estimate with OLS on the ages $x \in \{80, 81, \ldots, 90\}$. The estimates for $(\phi_1^{i,t}, \phi_2^{i,t})$ are then used in (9) to close the generated mortality scenario for ages $x > 90$.

Finally, we can switch to scenarios for future mortality rates using the transformation in (1), thus

$$q^i_{x,t} \quad = \quad 1 - \exp\left(-\mu^i_{x,t}\right), \tag{11}$$

for $t = 2020, 2021, \ldots, t_{\max}$ and $x \in 0, 1, \ldots, 120$.

3 Results, backtests and applications

3.1 Fitted and simulated mortality rates

Figure 9 shows the calibration of $q_{x,t}$ for Belgian males and a selection of ages $x \in \{25, 45, 65, 85\}$. Figure 10 shows the corresponding results for females. We show the median and 99% pointwise confidence intervals based on 10 000 scenarios of projected mortality rates. The black dots in this Figure are the observed mortality rates $q_{x,t}$ over the calibration period $\{1988, \ldots, 2019\}$. The dotted line indicates the mortality rates fitted with the model specified in Section 2.3. As a reference line we add the projection 2019-2070 of Federaal Planbureau (2020) ([FPB]).[14] The $q_{x,t}$'s in the FPB table are defined at *age in completed years* and have been transformed to $q_{x,t}$'s at exact age, using the transformation documented in Jaumain and Vandeschrick (2012).[15] The FPB model is a deterministic model, and its calibration does not follow the nowadays standard assumption of Poisson likelihood for the number of deaths. The projection of FPB is using the calibration period 1991-2018, whereas earlier projections of the FPB were using a calibration period starting in 1970.[16]

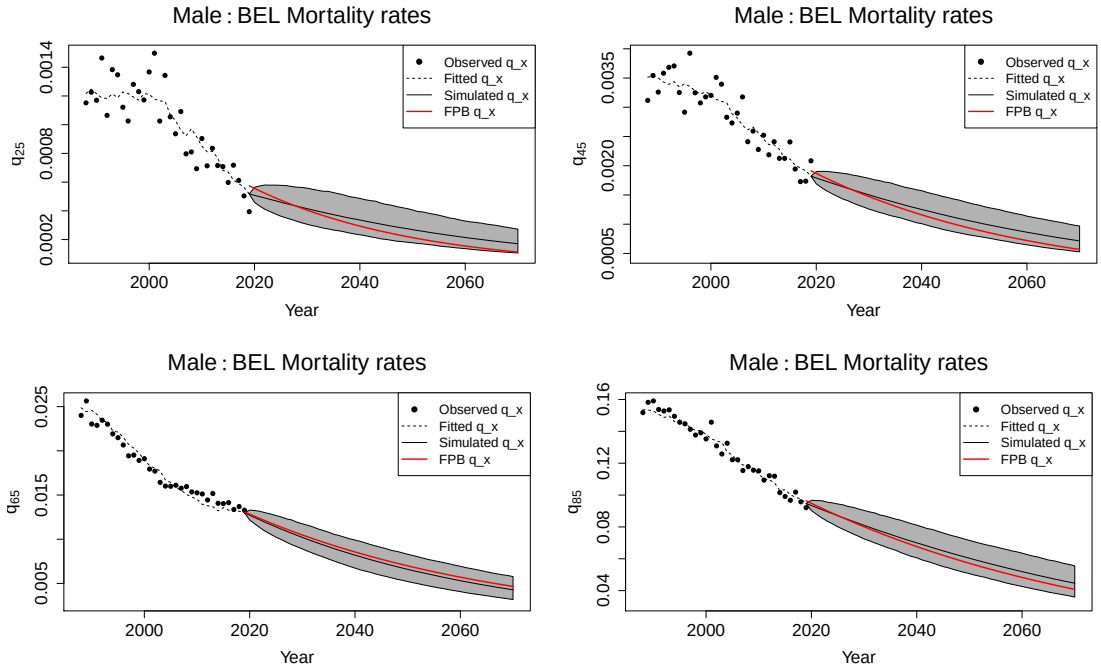

Figure 9: Estimated and projected mortality rates, $\hat{q}_{x,t}$, for Belgium, male data, ages 25, 45 (top row) and 65, 85 (bottom row), calibration period 1988-2019, projection 2020-2070. We plot 0.5% quantile, median and 99.5% quantile obtained from 10 000 simulations.

[14] We use the *Prospectieve sterftequotiënten 2019-2070* available on `https://www.plan.be/databases/database_det.php?lang=nl&ID=50` (tab `Qx-M` and `Qx-F` in the excel file `qx_bel_nl.xlsx`). The methodology is described in Federaal Planbureau (2009).

[15] We use formula (6) and (9) on page 11 of Jaumain and Vandeschrick (2012).

[16] See Federaal Planbureau (2009) on page 2.

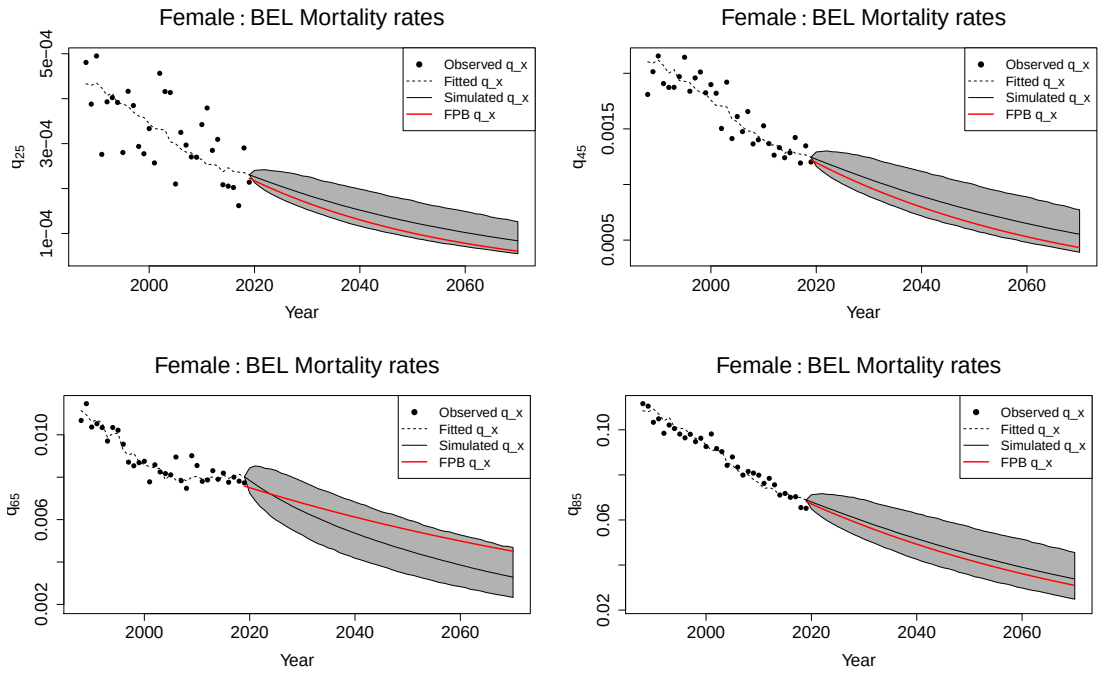

Figure 10: Estimated and projected mortality rates, $\hat{q}_{x,t}$, for Belgium, female data, ages 25, 45 (top row) and 65, 85 (bottom row), calibration period 1988-2019, projection 2020-2070. We plot 0.5% quantile, median and 99.5% quantile obtained from 10 000 simulations.

3.2 The IA|BE 2020 mortality projection for Belgium

The projected mortality table obtained with the best estimates of future $(K_t^M, \kappa_t^M, K_t^F, \kappa_t^F)$ (with $t = 2020, 2020, \ldots, 2070$) is the resulting 'IA|BE 2020 mortality projection for the Belgian population'. These best estimates for the period effects result from (5) and (6) with noise terms $\varepsilon_t^M = 0 = \delta_t^M$ and $\varepsilon_t^F = 0 = \delta_t^F$ for all future t. We close the mortality table obtained in this way with Kannisto (1994) such that $\mu_{x,t}$ for $x \in \{0, 1, \ldots, 120\}$ and $t \in \{2020, \ldots, 2070\}$ result. The corresponding mortality rates $q_{x,t}$ follow from (1). This table is available online for males and females.

3.3 Life expectancy: period and cohort

From the simulated scenarios for future mortality rates we obtain simulations for the period as well as cohort life expectancy. Using the assumption of piecewise constant force of mortality, the period life expectancy for an x year old in year t is

$$e_x^{\text{per}}(t) \quad = \quad \frac{1 - \exp\left(-\mu_{x,t}\right)}{\mu_{x,t}} + \sum_{k \geqslant 1} \left(\prod_{j=0}^{k-1} \exp\left(-\mu_{x+j,t}\right) \right) \frac{1 - \exp\left(-\mu_{x+k,t}\right)}{\mu_{x+k,t}}, \tag{12}$$

and the cohort life expectancy for an x year old in year t is

$$e_x^{\text{coh}}(t) \quad = \quad \frac{1 - \exp\left(-\mu_{x,t}\right)}{\mu_{x,t}} + \sum_{k \geqslant 1} \left(\prod_{j=0}^{k-1} \exp\left(-\mu_{x+j,t+j}\right) \right) \frac{1 - \exp\left(-\mu_{x+k,t+k}\right)}{\mu_{x+k,t+k}}, \tag{13}$$

see, for example, Pitacco et al. (2009). Using the mortality scenarios generated as described in Section 2.5 we obtain simulations of the period and cohort life expectancy, say $e_x^{\text{per},i}(t)$ and $e_x^{\text{coh},i}(t)$. Scenarios can be generated beyond 2070. Thus, when calculating life expectancies in, for example, 2070, we will project the mortality rates for 120 years after 2070. To construct a point estimate for the period and cohort life expectancy, we use the best estimate table introduced in Section 3.2.

Figure 11 shows the observed period life expectancy (black dots) for a 0 (left) and 65 (right) year old male (top panels), the calibrated period life expectancy (red line) and the simulations of $e_0(t)$ and $e_{65}(t)$ for $t = 2020, \ldots, 2070$. The blue fan chart shows the cohort life expectancy, $e_0^{\text{coh}}(t)$ and $e_{65}^{\text{coh}}(t)$. The corresponding results for females are shown in the bottom panels of Figure 11.

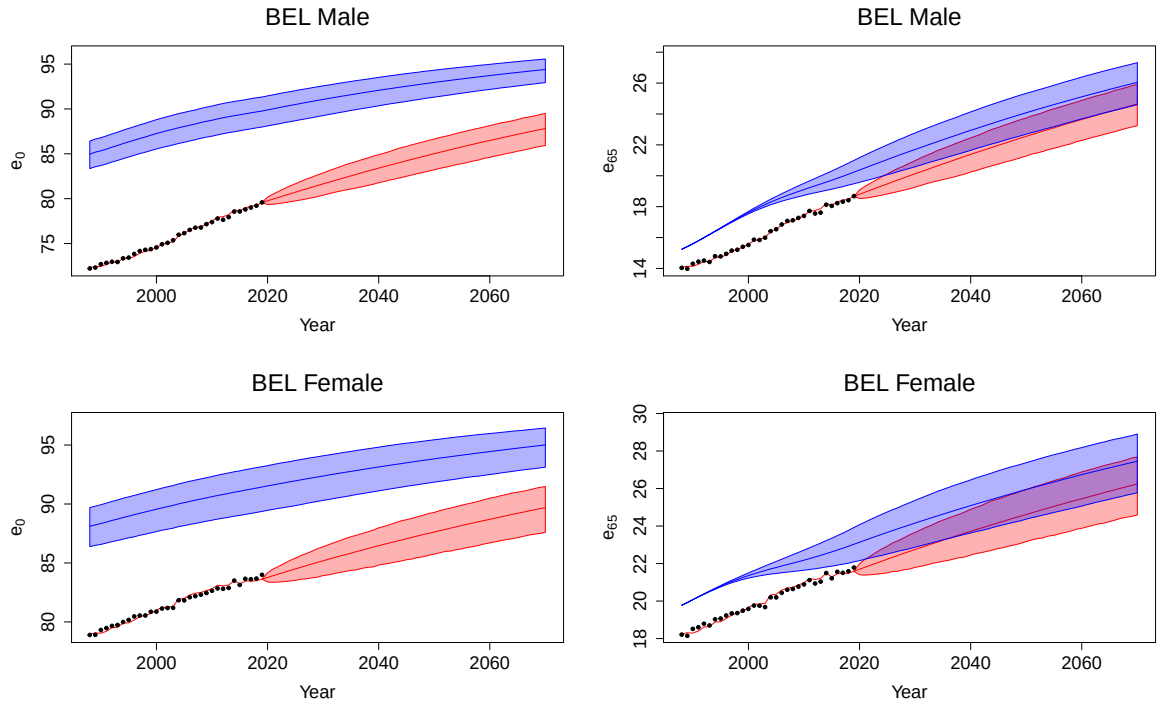

Figure 11: Period (black dots and red lines) and cohort (blue) life expectancy for a 0 year old (left) and 65 year old (right), male (top) and female (bottom) data. Mortality model calibrated on male and female data, ages 0-90, years 1988-2019 and closed with method of Kannistö. We plot 0.5% quantile, median and 99.5% quantile obtained from 10 000 simulations.

Table 2 lists the median and 99% confidence intervals of $e_x^{\text{coh}}(t)$ for some specific choices of x and t. As a benchmark the table also shows the cohort life expectancies published by Federaal Planbureau (2020).[17] We transform these from *ages in completed years* to exact ages, using Jaumain and Vandeschrick (2012).[18]

Inspired by Koninklijk Actuarieel Genootschap (2016, 2018, 2020), the top panels of Figure 12 show the projected period and cohort expected age at death ($x + E[T_x]$) of a Belgian male in

[17] This is the `GLEX_Bel_Nl.xlsx`-file at https://www.plan.be/databases/data-50-nl-prospectieve+sterfte quotienten+2019+2070.

[18] We use formulas (11) and (14).

year		males		females	
		0	65	0	65
2020	Best Est.	89.91	20.38	91.54	23.14
	$[q_{0.5}; q_{50}; q_{99.5}]$	[88.11;89.89;91.46]	[19.57;20.37;21.17]	[89.46;91.53;93.25]	[22.15;23.14;24.07]
	FPB	(90.07;90.25)	(20.11;20.56)	(91.28;91.53)	(22.92;23.38)
2040	Best Est.	92.08	22.94	93.15	25.09
	$[q_{0.5}; q_{50}; q_{99.5}]$	[90.35;92.08;93.52]	[21.65;22.94;24.14]	[91.12;93.14;94.82]	[23.63;25.09;26.46]
	FPB	(92.09;92.36)	(22.80;23.26)	(92.80;93.08)	(24.82;25.28)
2060	Best Est.	93.73	25.11	94.45	26.74
	$[q_{0.5}; q_{50}; q_{99.5}]$	[92.18;93.72;94.97]	[23.69;25.11;26.39]	[92.50;94.45;95.97]	[25.06;26.74;28.18]
	FPB	(93.62;93.90)	(25.00;25.48)	(94.06;94.34)	(26.45;26.92)

Table 2: Cohort life expectancy for a 0 and 65 year old, Best Estimate and 0.5% quantile, median and 99.5% quantile obtained from 10 000 simulations, males and females. 'FPB' refers to Federaal Planbureau (2020); the first number is the cohort life expectancy as published in Federaal Planbureau (2020) (i.e. using *ages in completed years*) and the second number is the cohort life expectancy at exact ages, using the transformations proposed in Jaumain and Vandeschrick (2012).

the year 2020 and 2040. The corresponding results for females are given in the bottom panels of Figure 12. First of all, the uncertainty in the predicted expected ages at deaths decreases with higher ages. This is because the higher the age, the less far in the future we have to project the mortality rates. Second, the projected cohort expected age at death decreases until the age of about 60 years. The reason is that younger persons benefit more from the lower projected future mortality rates. Afterwards, the cohort expected age at death again increases due to the fact that older people already survived up to a certain high age. Third, the period expected age at death increases over the whole age range. This is in line with our intuitions since we only use projected mortality rates at one specific year. Last, the confidence bounds capture only the uncertainty in the future mortality rates and do not look at one particular individual. Hence, the narrow confidence bounds at high ages do not imply that we can accurately predict the moment at which one particular individual will die.

3.4 Back testing the mortality model

One of the evaluation criteria used in the process of selecting a mortality model, is the performance of a model in back tests (see Cairns et al. (2009)). We illustrate the performance of the IA|BE 2020 mortality projection model in two types of back tests. In Figure 13 (females) and 14 (males) we calibrate the model on data from 1988 to 2011 and use it to project mortality rates $q_{x,t}$ with $t \in \{2012, \ldots, 2019\}$.

Figure 15 visualizes the results of three back tests, on calibration periods $\{1988, \ldots, 2000\}$, $\{1988, \ldots, 2005\}$ and $\{1988, \ldots, 2010\}$, expressed as fitted values and projections of the period life expectancy for a 0 year old and a 65 year old. All three back tests perform well for females. The observed period life expectancies always fall within the fan charts. The back test for males on the smallest calibration period $\{1988, \ldots, 2000\}$ performs clearly worse than the other back tests.

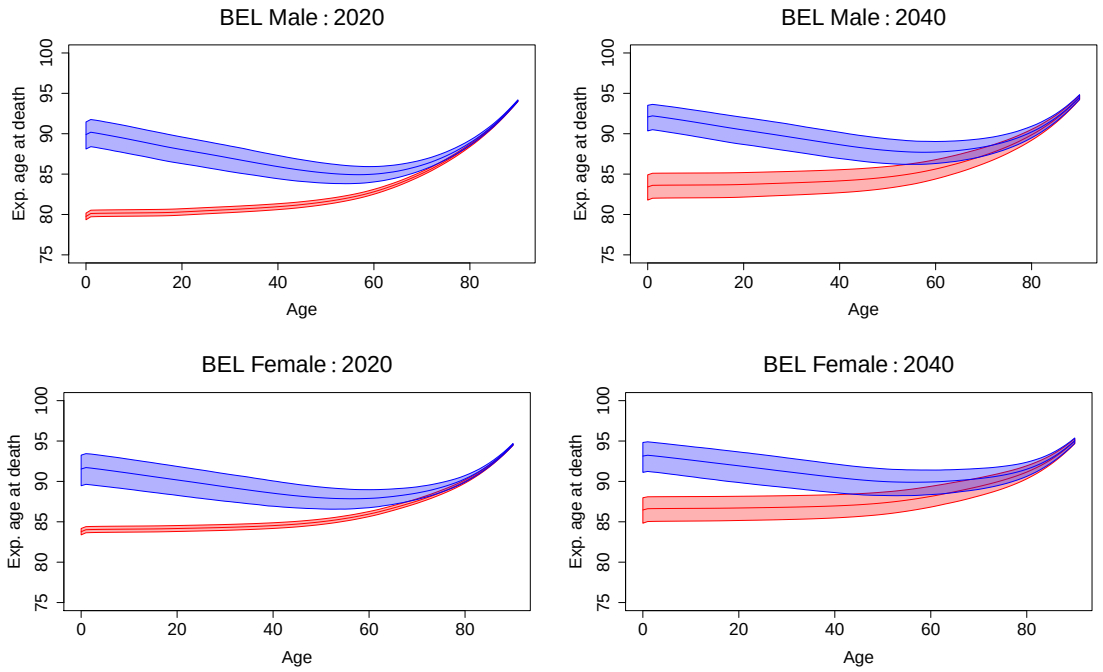

Figure 12: Period (red) and cohort (blue) expected age at death for a Belgian male (top) and female (bottom) in 2020 (left) and 2040 (right). We plot 0.5% quantile, median and 99.5% quantile obtained from 10 000 simulations.

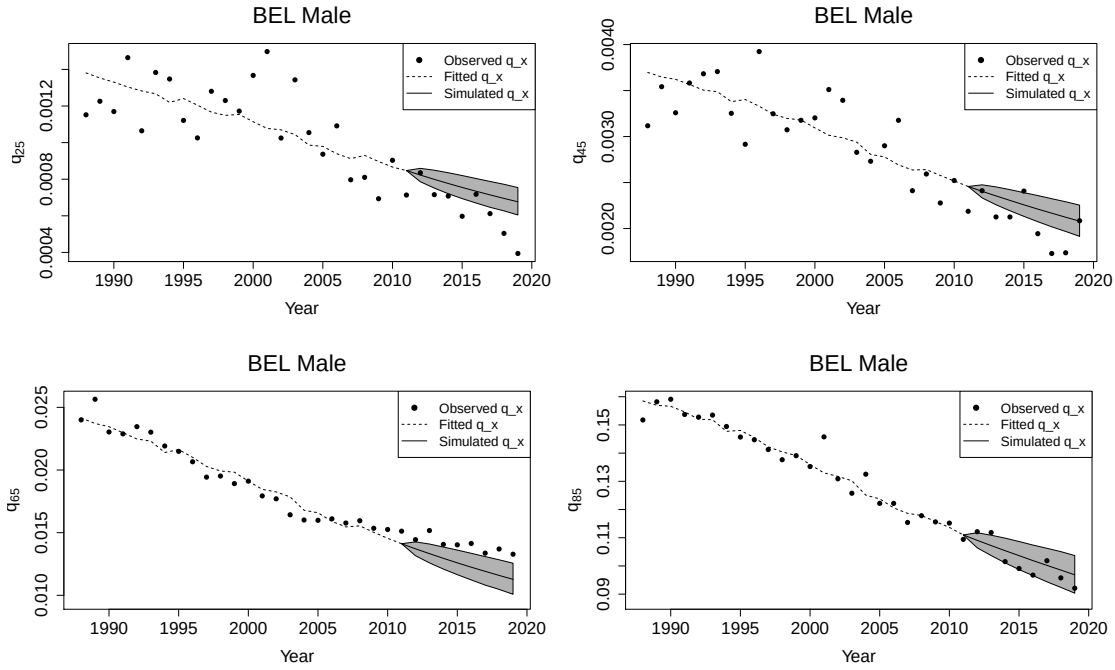

Figure 13: Back test on $q_{x,t}$, for Belgium, male data, ages 25, 45 (top row) and 65, 85 (bottom row). We calibrate on 1988-2011 data and then project 2012-2019. We plot 0.5%, median and 99.5% quantile obtained from 10 000 simulations.

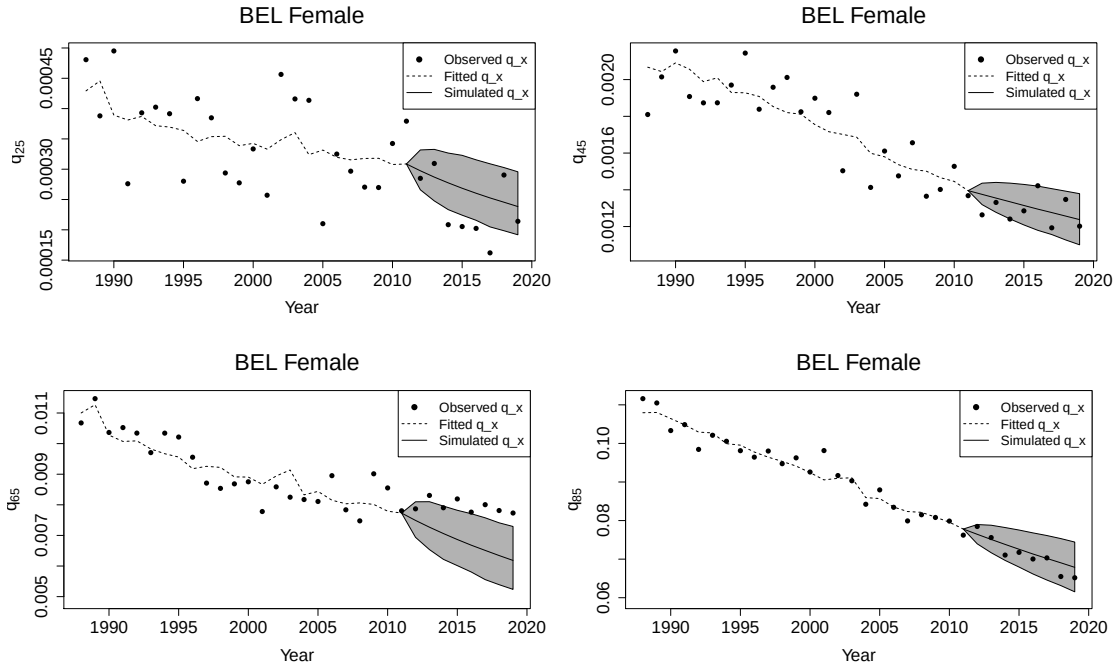

Figure 14: Back test on $q_{x,t}$, for Belgium, female data, ages 25, 45 (top row) and 65, 85 (bottom row). We calibrate on 1988-2011 data and then project 2012-2019. We plot 0.5%, median and 99.5% quantile obtained from 10 000 simulations.

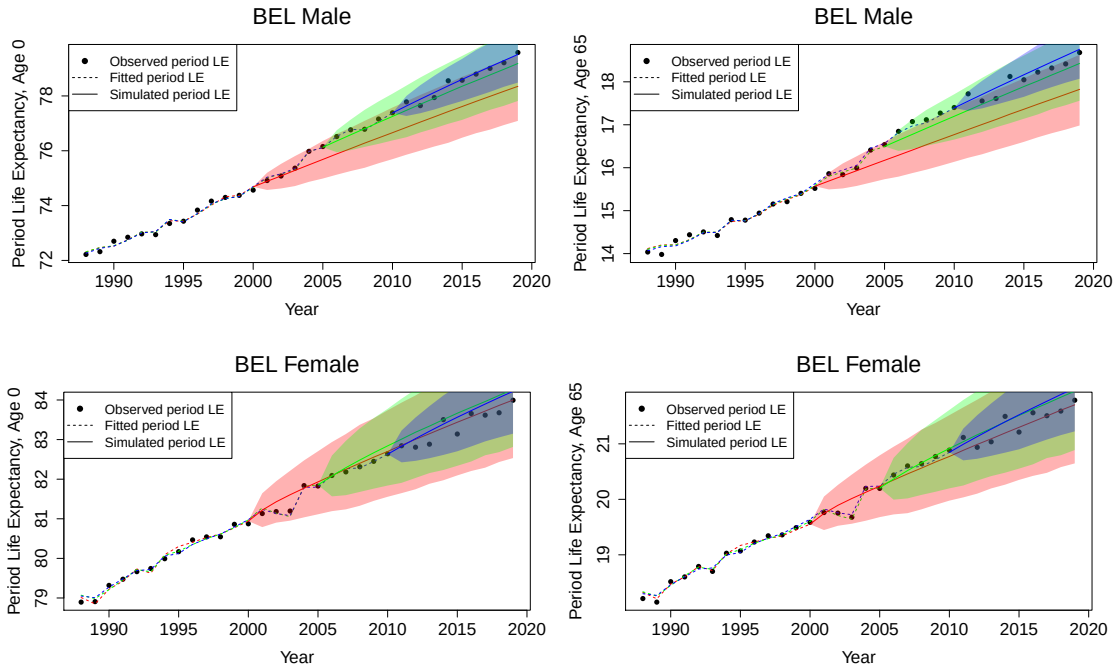

Figure 15: Back tests using calibration periods 1988-2000 (red), 1988-2005 (green) and 1988-2010 (blue), period life expectancy for a 0 year old (left) and 65 year old (right), male (top) and female (bottom) data. We plot 0.5%, median and 99.5% quantile obtained from 10 000 simulations.

4 From IA|BE 2015 to IA|BE 2020: changes and impact assessment

Compared to the IA|BE 2015 model, IA|BE 2020 is calibrated on an updated and slightly changed data set (as discussed in Section 2.2), while accounting for some methodological changes. Table 3 quantifies the impact of these various changes in line with Koninklijk Actuarieel Genootschap (2020). Our starting point in this table is the cohort life expectancy in 2020 as estimated along the principles of IA|BE 2015. However, we rely on the data collected in 2020 and restrict the calibration period to the year 2013 for Belgium and to the year 2009 for the other European countries. These were the end years of the calibration period used in IA|BE 2015. Therefore, the numbers in the row 'IA|BE 2015' in Table 3 are slightly different from the numbers reported in Antonio et al. (2015)

Cohort LE 2020	males		females	
	0	65	0	65
IA|BE 2015	88.71	19.92	92.85	23.63
Update EU 2013	0.45	0.17	-0.25	-0.13
Shorten Cal. Per.	0.94	0.34	-0.87	-0.19
Joint estimation	-0.13	-0.00	-0.01	0.07
Adding intercept	0.46	0.12	0.29	0.03
EU 2013 - BEL 2014	0.06	0.05	0.15	0.17
EU 2014 - BEL 2014	0.50	0.25	0.57	0.28
EU 2014 - BEL 2015	-0.06	-0.08	-0.13	-0.20
EU 2015 - BEL 2015	-0.82	-0.37	-0.89	-0.40
EU 2015 - BEL 2016	0.02	0.02	0.05	0.06
EU 2016 - BEL 2016	0.13	0.07	0.22	0.10
EU 2016 - BEL 2017	-0.02	-0.01	-0.07	-0.08
EU 2017 - BEL 2017	-0.19	-0.09	-0.20	-0.07
EU 2017 - BEL 2018	0.00	0.01	0.03	-0.03
EU 2018 - BEL 2018	-0.32	-0.16	-0.24	-0.09
EU 2018 - BEL 2019	0.16	0.14	0.05	-0.01
IA|BE 2020	89.91	20.38	91.54	23.14

Table 3: Changes in the estimated cohort life expectancies due to the transition from the IA|BE 2015 to the IA|BE 2020 model.

The row 'Update EU 2013' in Table 3 refers to the availability of data up to 2013 for all the 14 European countries that are used in the calibration. So, compared to the previous row, we extend the European mortality data set with the data points corresponding to the years 2010-2013. 'Shorten Cal. Per.' means that we shorten the calibration periods by changing the start year to 1988. Further, 'Joint estimation' refers to the joint modelling of the time series dynamics for men and women, namely $(K_t^M, \kappa_t^M, K_t^F, \kappa_t^F)$. Thereafter we add the intercept term to the Belgian period effect κ_t^M and κ_t^F ('Adding intercept'). Finally, we consecutively extend the European and Belgian data set with incremental years of data. This stepwise extension of the data set with a newly observed data point reflects the reality of recalibrating the model on an update of the data set. More specifically, mortality data for all the European countries for year t is published on Eurostat and HMD around the beginning of year $t+2$. In August / September of year $t+2$ Statbel provides new mortality data for Belgium for year $t+1$.

In conclusion, shortening the calibration period has the greatest impact on the estimated cohort life expectancy in the year 2020. Another large impact can be observed when adding data for

Europe for the year 2015. In general the cohort life expectancy for male newborns has increased with more than one year, when stepping from the IA|BE 2015 to the IA|BE 2020 forecast. In the case of females, there is a decrease with about 1.3 years.

5 Conclusion

This report describes the methodology used to produce the IA|BE 2020 mortality projection as well as the stochastic model underneath this best estimate table. The mortality model is of Li & Lee type and uses Belgian data, together with mortality data from a set of 13 other well selected European countries, to forecast mortality. Actuaries can use this model to generate scenarios for future mortality, or they can use the table of $q_{x,t}$'s as a best estimate scenario of future mortality. We selected this model from a comparative study of a wide set of stochastic mortality models published in recent literature. The model performs well in terms of (among others) robustness, biological reasonableness, transparency, in sample fit and back testing.

Acknowledgements

Katrien Antonio gratefully acknowledges the insights acquired from the many discussions with prof. dr. Michel Vellekoop and dr. Frank Van Berkum related to research on mortality modelling.

References

Antonio, K. (2012). Sluiten van de periodetafel GBM/V 2005–2010. *www.ag-ai.nl*.

Antonio, K., Devolder, L., and Devriendt, S. (2015). The IA|BE 2015 mortality projection for the Belgian population. https://www.iabe.be.

Antonio, K., Devriendt, S., de Boer, W., de Vries, R., De Waegenaere, A., Kan, H.-K., Kromme, E., Ouburg, W., Schulteis, T., Slagter, E., et al. (2017). Producing the Dutch and Belgian mortality projections: a stochastic multi-population standard. *European actuarial journal*, 7(2):297–336.

Barrieu, P., Bensusan, H., Karoui, N. E., Hillairet, C., Loisel, S., Ravanelli, C., and Salhi, Y. (2012). Understanding, modelling and managing longevity risk: key issues and main challenges. *Scandinavian Actuarial Journal*, 3:203–231.

Brouhns, N., Delwarde, A., and Denuit, M. (2002a). Elaboration de tables de mortalité prospectives ou comment tarifer des rentes viagères lorsque la mortalité évolue. *KVBA-ARAB Report*.

Brouhns, N., Denuit, M., and Vermunt, J. K. (2002b). A Poisson log-bilinear regression approach to the construction of projected lifetables. *Insurance: Mathematics and economics*, 31(3):373–393.

Cairns, A., Blake, D., Dowd, K., Coughlan, G., Epstein, D., Ong, A., and Balevich, I. (2009). A quantitative comparison of stochastic mortality models using data from England and Wales and the United States. *North American Actuarial Journal*, 13(1):1–35.

Cairns, A. J., Blake, D., Dowd, K., and Kessler, A. R. (2016). Phantoms never die: living with unreliable population data. *Journal of the Royal Statistical Society: Series A (Statistics in Society)*, 179(4):975–1005.

Cox, B., Wuillaume, F., Van Oyen, H., and Maes, S. (2010). Monitoring of all-cause mortality in belgium (be-momo): a new and automated system for the early detection and quantification of the mortality impact of public health events. *International Journal of Public Health*, 55(4):251–259.

Delfosse, P. and Boelen, P. (2002). Conséquences pour les rentes viagères. *KVBA-ARAB Report*.

Doray, L. G. (2008). Inference for the logistic-type models for the force of mortality. *Living to 100 and beyond, SOA Monograph*, pages 1–18. M-LI*08-01*.

Federaal Planbureau (2009). Prospectieve sterftequotiënten per geslacht en uniseks. https://www.plan.be/uploaded/documents/201002040818570.wp200918.pdf.

Federaal Planbureau (2020). Prospectieve sterftequotiënten 2019-2070. https://www.plan.be/databases/data-50-nl-prospectieve+sterftequotienten+2019+2070.

Jaumain, C. and Vandeschrick, C. (2012). Sterftetafel: van verstreken leeftijden naar exacte leeftijden.

Kannisto, V. (1994). *Development of oldest-old mortality, 1950-1990: Evidence from 28 developed countries*. Odense University Press.

Koninklijk Actuarieel Genootschap (2014). Prognosetafel AG2014. https://www.ag-ai.nl.

Koninklijk Actuarieel Genootschap (2016). Prognosetafel AG2016. https://www.ag-ai.nl.

Koninklijk Actuarieel Genootschap (2018). Prognosetafel AG2018. https://www.ag-ai.nl.

Koninklijk Actuarieel Genootschap (2020). Prognosetafel AG2020. https://www.ag-ai.nl.

Lambrechts, K. (2001). Belgian mortality tables for the past and the next century. *KVBA-ARAB Report*.

Lee, R. and Carter, L. (1992). Modeling and forecasting the time series of US mortality. *Journal of the American Statistical Association*, 87:659–671.

Li, J. (2013). A Poisson common factor model for projecting mortality and life expectancy jointly for females and males. *Population Studies: A Journal of Demography*, 67(1):111–126.

Li, N. and Lee, R. (2005). Coherent mortality forecasts for a group of populations: an extension of the Lee–Carter method. *Demography*, 42(3):575–594.

Pitacco, E., Denuit, M., Haberman, S., and Olivieri, A. (2009). *Modeling Longevity Dynamics for Pensions and Annuity Business*. Oxford University Press, London.

A Data sources

Country	2015	2016	2017	2018	2019	Last mod. HMD	Last mod. EURO1	Last mod. EURO2
Austria	HMD	HMD	HMD	EURO		3 Sep. 2018	3 July 2020	3 July 2020
Belgium	HMD	HMD	HMD	HMD	STAT	6 Sep. 2019	-	-
Denmark	HMD	HMD	HMD	HMD	HMD	20 Mars 2020	-	-
Finland	HMD	HMD	HMD	HMD	HMD	10 Sep. 2020	-	-
France[19]	HMD	HMD	HMD	HMD		29 Aug. 2020	-	-
Germany ($\geqslant$ 1990)	HMD	HMD	HMD	EURO		17 Dec. 2018	3 July 2020	3 July 2020
Iceland	HMD	HMD	HMD	HMD		2 April 2020	-	-
Ireland	HMD	HMD	HMD	EURO		1 Oct. 2019	3 July 2020	3 July 2020
Luxembourg	HMD	HMD	HMD	EURO		10 Dec. 2019	3 July 2020	3 July 2020
Netherlands	HMD	HMD	HMD	HMD		3 April 2020	-	-
Norway	HMD	HMD	HMD	HMD		21 Nov. 2019	-	-
Sweden	HMD	HMD	HMD	HMD		9 Jan. 2020	-	-
Switzerland	HMD	HMD	HMD	HMD		8 May 2020	-	-
United Kingdom	HMD	HMD	HMD	HMD		11 July 2020	-	-
West Ger. ($<$ 1990)						17 Dec. 2018	-	-

Table 4: The data sources for each country and for each year. The data source for years before 2015 is HMD. Further, we list the date of last modifications of each of the databases as consulted when writing this report. EURO1 refers to the databases from Eurostat about the period and cohort number of deaths, EURO2 refers to the database from Eurostat about the population sizes at the start of the year. STAT refers to the source Statbel or Statistics Belgium.

B Choice of the calibration period to achieve a stable AR(1) process

In this appendix we discuss the instability of the AR(1) process, used to model the male Belgian period effect κ_t^M in Equation (6), when considering the calibration period $\bar{\mathcal{T}} = \{1970, ..., 2018\}$ for the common European mortality trend and the calibration period $\mathcal{T} = \{1970, ..., 2019\}$ for the Belgian deviation of this common trend. Afterwards, we provide a solution by shortening the calibration period to achieve stability.

First, we visualize the parameter estimates in the calibrated mortality model for male data in Figure 3 (European parameters: $\hat{A}_x$, $\hat{B}_x$ and $\hat{K}_t$) and Figure 4 (Belgian parameters: $\hat{\alpha}_x$, $\hat{\beta}_x$ and $\hat{\kappa}_t$). Figures 5 and 6 show the same results for females.

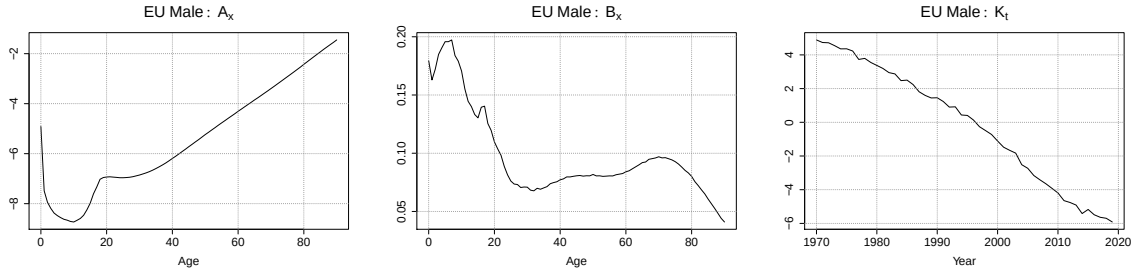

Figure 16: Estimated common parameters, male data, ages 0-90, years 1970-2019: $\hat{A}_x$, $\hat{B}_x$ and $\hat{K}_t$.

[19] Whenever data is extracted on Eurostat for France, we exclude deaths that occurred in overseas departments (Guadeloupe, Martinique, Guyane, La Réunion and Mayotte) to be consistent with the HMD population figures. Thus, we extract data for Metropolitan France on Eurostat.

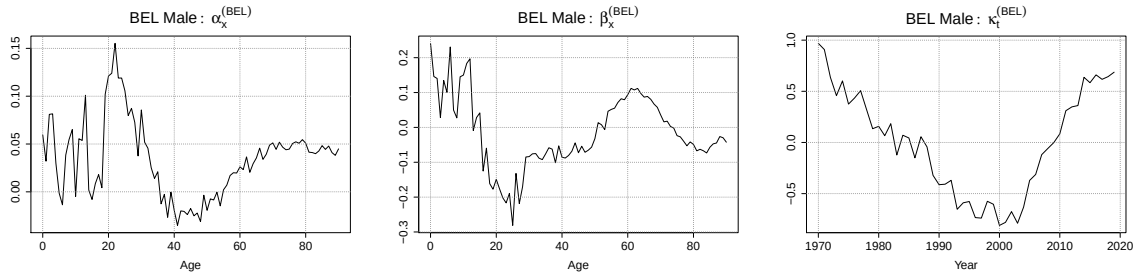

Figure 17: Estimated parameters for Belgium, male data, ages 0-90, years 1970-2019: $\hat{\alpha}_x$, $\hat{\beta}_x$ and $\hat{\kappa}_t$.

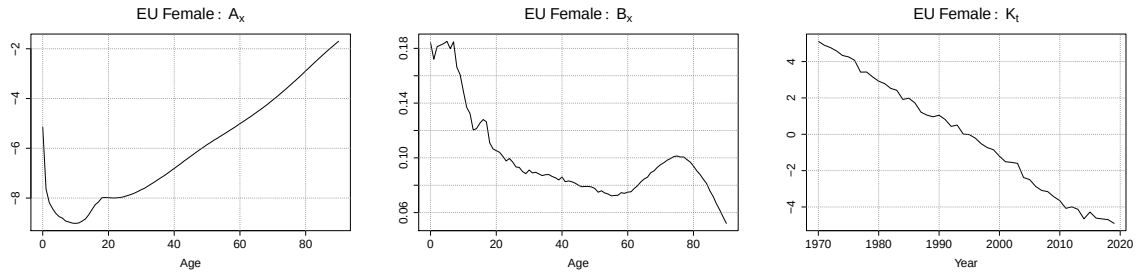

Figure 18: Estimated common parameters, female data, ages 0-90, years 1970-2019: $\hat{A}_x$, $\hat{B}_x$ and $\hat{K}_t$.

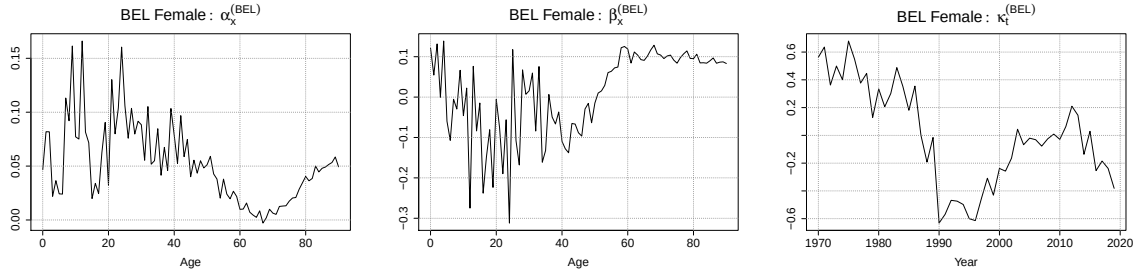

Figure 19: Estimated parameters for Belgium, female data, ages 0-90, years 1970-2019: $\hat{\alpha}_x$, $\hat{\beta}_x$ and $\hat{\kappa}_t$.

Next, we document the parameter estimates in the time series specifications (see Equations (5) and (6)) in Table 5. The parameter estimate $\hat{\phi}^M$ in the AR(1) time series model for $\hat{\kappa}_t^M$ exceeds 1, leading to an unstable process. These values would lead to a divergence of the Belgian mortality trend from the European mortality trend, a scenario that we consider as implausible.

One possible solution to this problem exists in shortening the original calibration periods $\bar{\mathcal{T}} = \{1970, ..., 2018\}$ (European trend) and $\mathcal{T} = \{1970, ..., 2019\}$ (Belgian deviation trend) in a simultaneous way. Figure 20 depicts the estimates $\hat{\phi}$ for different start years t in both calibration periods $\bar{\mathcal{T}}$ and $\mathcal{T}$. The plot shows the stability of the female AR(1) process over all examined calibration periods. The AR(1) process for males becomes stable for the calibration period with start year 1982. However, the process becomes again unstable for later start years as the parameter estimate only dips below one locally.

	$\hat{\theta}^{(BEL)}$	$\hat{c}^{\text{BEL}}$	$\hat{\phi}^{(BEL)}$		$\hat{C}^{(BEL)}$			
					ε_t^M	δ_t^M	ε_t^F	δ_t^F
Male	-0.2205	-0.0055	1.0193	ε_t^M	0.0291	-0.0139	0.0322	0.0044
				δ_t^M	-0.0139	0.0228	-0.0139	-0.0058
Female	-0.2044	-0.0184	0.8849	ε_t^F	0.0322	-0.0139	0.0410	0.0059
				δ_t^F	0.0044	-0.0058	0.0059	0.0288

Table 5: Time series parameter estimates using European and Belgian data, male and female data, ages 0-90, calibration periods $\bar{\mathcal{T}} = \{1970, ..., 2018\}$ (European mortality trend) and $\mathcal{T} = \{1970, ..., 2019\}$ (Belgian deviation trend) .

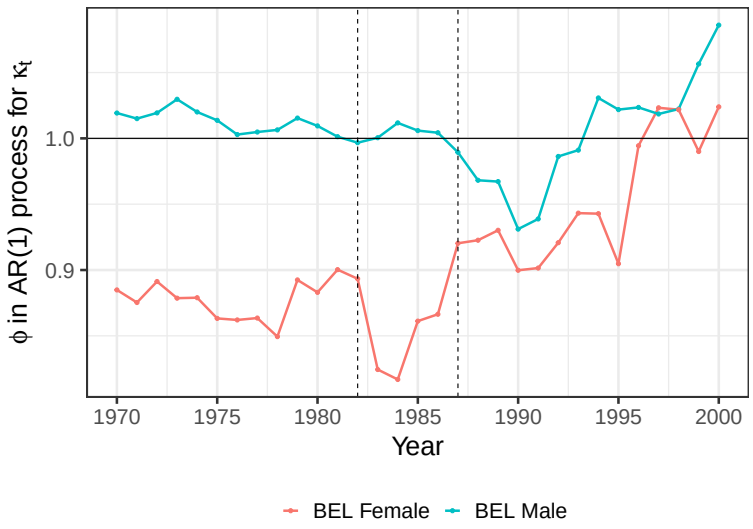

Figure 20: The parameter estimates $\hat{\phi}$ in the time series of the Belgium-specific period effect κ_t for calibration periods $\bar{\mathcal{T}}$ and $\mathcal{T}$ with the start year t varying from 1970 to 2000 for the Belgian males (blue line) and females (red line).

We want the choice for the start year of the calibration periods $\bar{\mathcal{T}}$ and $\mathcal{T}$ to be a stable choice in light of future updates of the model. Figure 21 therefore repeats the experiment from Figure 20, but we let the end years of both calibration periods vary. E.g., the golden line `15-16` means that we fix the end year of the calibration period $\bar{\mathcal{T}}$ for the European mortality trend to 2015 and the one for the Belgian deviation of this European trend to 2016. In particular, we act as if we were in the past and are confronted with the same problem as in Figure 20. We observe an overall stable area for males with start years between 1988 and 1991. In the female case, no problems occur. Therefore our final selected calibration periods are $\bar{\mathcal{T}} = \{1988, ..., 2018\}$ (European mortality trend) and $\mathcal{T} = \{1988, ..., 2019\}$ (Belgian deviation trend).

With the start year of the calibration periods $\bar{\mathcal{T}}$ (European mortality trend) and $\mathcal{T}$ (Belgian deviation trend) fixed to 1988, we now investigate if the calibration period $\bar{\mathcal{T}}$ for the European mortality trend can possibly be extended, while safeguarding the stability of the AR(1) process. We show the results in Figure 22 for some variable end years. Each line in this figure shows the parameter estimate $\hat{\phi}$ in the time series of the male Belgian period effect $\hat{\kappa}_t$ with the start year in the calibration period for the European mortality trend varying between 1970 and 1988 and with some specific end years, indicated by the legend labels. The start year of the calibration

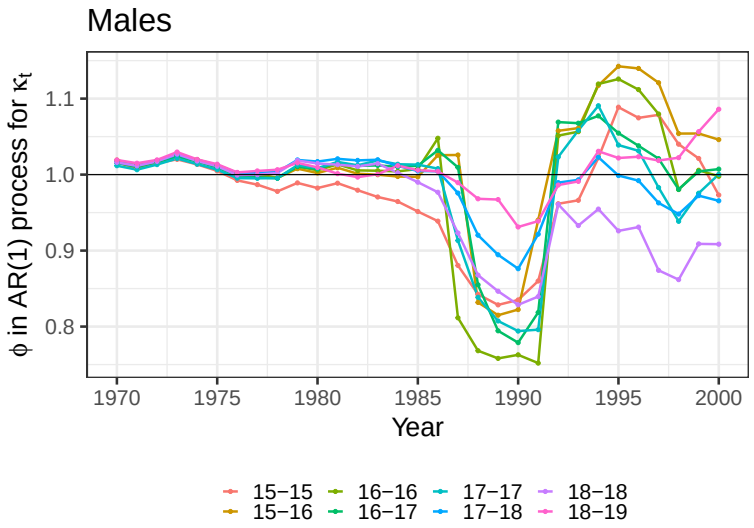

Figure 21: The parameter estimates $\hat{\phi}$ in the time series of the estimated Belgian period effect $\hat{\kappa}_t$ for calibration periods $\bar{\mathcal{T}}$ and $\mathcal{T}$ with the start year t varying from 1970 to 2000 and with varying end years, for the Belgian males.

period for the Belgian deviation stays fixed at the year 1988. We can not find a stable region as was the case in Figure 21. Therefore, we continue with the earlier selected calibration periods $\bar{\mathcal{T}} = \{1988, ..., 2018\}$ (European mortality trend) and $\mathcal{T} = \{1988, ..., 2019\}$ (Belgian deviation).

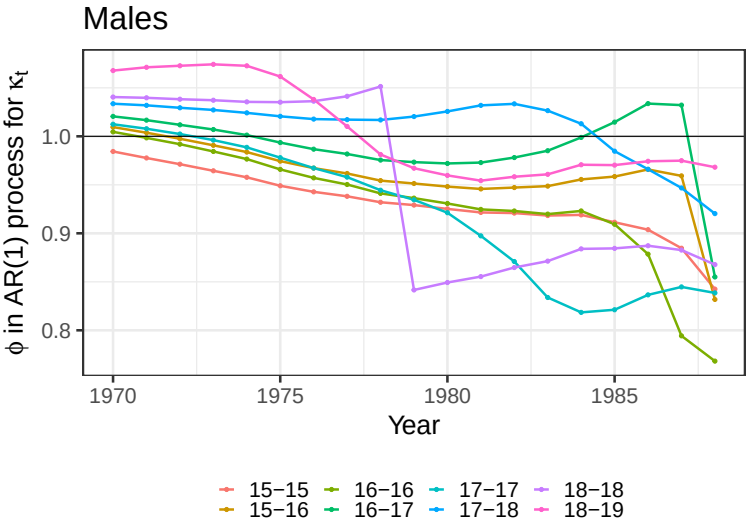

Figure 22: The parameter estimates $\hat{\phi}$ in the time series of the estimated Belgian period effect $\hat{\kappa}_t$ for calibration periods $\bar{\mathcal{T}}$ and $\mathcal{T}$ with the start year t in $\bar{\mathcal{T}}$ (European trend) varying from 1970 to 2000 and with varying end years, for the Belgian males. Note that we fix the start year of the calibration period $\mathcal{T}$ to 1988.

C AR(k)-process for Belgian period effect κ_t

C.1 Description, calibration and projection

We also investigate the effect of an increase of the order of the autoregressive time series process for the male Belgian deviation κ_t^M from the European mortality trend. This strategy has the advantage that we do not intervene in the start year of the calibration period. We simply increase the lag-order of the AR(k) process until we reach a stable process.

First, we calibrate the mortality model on ages 0-90 and calibration periods 1970-2018 (European trend) and 1970-2019 (Belgium deviation) for males and females separately, using the approach explained in Section 2.4. This results in estimated parameters of the LL mortality model, namely $\hat{A}_x, \hat{B}_x, \hat{K}_t, \hat{\alpha}_x, \hat{\beta}_x$ and $\hat{\kappa}_t$, for each gender.

Stability of an AR(k) process. An autoregressive process of lag-order k, in short an AR(k) process, is written as

$$\kappa_t = a_1\kappa_{t-1} + a_2\kappa_{t-2} + \ldots + a_k\kappa_{t-k} + \delta_t,$$

for $t \geqslant k$. This process is stable whenever the roots of its characteristic polynomial

$$\phi(x) = 1 - a_1x - a_2x^2 - \ldots - a_kx^k$$

all lie outside the unit circle. Whenever one root is less than 1 in absolute value, κ_t diverges as time moves on. Eventually, this would lead to unstable mortality projections, i.e. divergence from the European mortality trend.

Section 2.5 already reveals that an AR(1) process will not be sufficient to model the estimated male Belgian period effect $\hat{\kappa}_t^M$. Therefore, we increase the lag order until we get a stable process for $\hat{\kappa}_t^M$. Since we do not observe stability issues for the AR(1) process to model the female Belgian period effect $\hat{\kappa}_t^F$, we keep its lag order at one. Finally, we retrieve the following time series dynamics

$$\begin{aligned}\hat{\kappa}_t^M &= 0.0027 + 0.9712\hat{\kappa}_{t-1}^M - 0.0255\hat{\kappa}_{t-2}^M + 0.3916\hat{\kappa}_{t-3}^M - 0.0711\hat{\kappa}_{t-4}^M - 0.2951\hat{\kappa}_{t-5}^M + \delta_t^M,\\ \hat{\kappa}_t^F &= -0.0184 + 0.8834\hat{\kappa}_{t-1}^F + \delta_t^F.\end{aligned}$$

Figure 23 indicates that the roots of the corresponding characteristic polynomials all lie outside the unit circle. We plot the inverse roots for visualization purposes. Hence, both processes are stable.

Generating future scenarios of mortality. Next, we can project the time-dependent parameters K_t^M, κ_t^M, K_t^F and κ_t^F in a similar way as explained in Section 2.5. However, we now project from an AR(5) instead of an AR(1) process for males, as described and estimated in the previous paragraph. We again generate 10 000 scenarios and show the corresponding fan charts in Figure 24. We make a comparison with the earlier discussed projection for the model that uses AR(1) processes for both κ_t^M and κ_t^F and was calibrated on the shorter period starting in the year 1988 (see Figure 8). For the males, we observe a higher uncertainty, i.e. wider fan chart, for the model that uses the longer calibration period, starting from 1970 on.

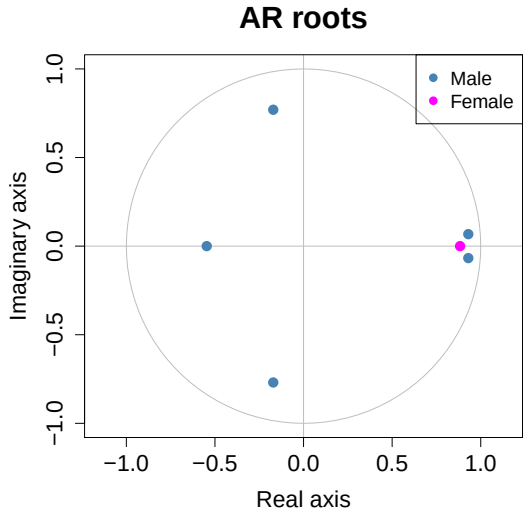

Figure 23: The inverse roots of the characteristic polynomials of the AR(k) processes for $\hat{\kappa}_t^M$ and $\hat{\kappa}_t^F$. Based on the mortality model, calibrated on ages 0-90 and years 1970-2019.

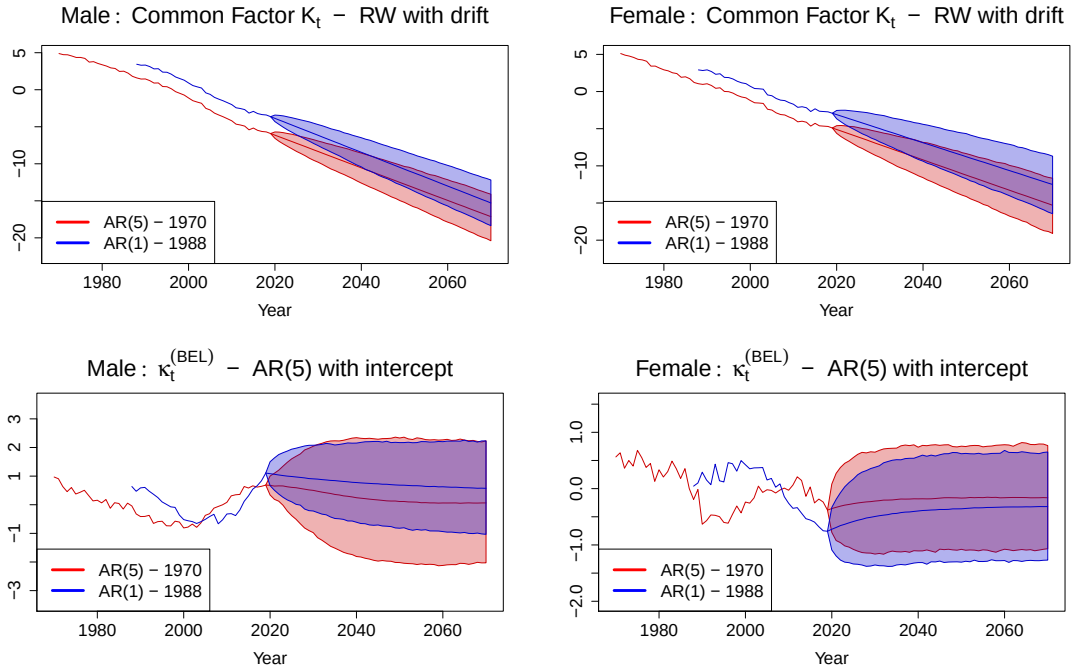

Figure 24: Projection of time dependent parameters: K_t and κ_t, male (left) and female (right) data. We plot 0.5% quantile, median and 99.5% quantile obtained from 10 000 simulations. We add the projection results of Figure 8 in blue. The legend label `AR(5)-1970` refers to the mortality model, calibrated on ages 0-90 and years 1970-2018 (European trend) and 1970-2019 (Belgian deviation), and that uses an AR(5) to attain stability for the time series of κ_t^M and an AR(1) process for κ_t^F. The legend label `AR(1)-1988` refers to the mortality model, calibrated on ages 0-90 and years 1988-2018 (European trend) and 1988-2019 (Belgian deviation), and that uses an AR(1) processes for both κ_t^M and κ_t^F (Sections 2 and 3).

C.2 Fitted and simulated mortality rates

We repeat the procedure explained in Section 3.1 and construct fitted and simulated mortality rates with the AR(5) and AR(1) model for the male and female Belgian deviation respectively. Figures 25 (males) and 26 (females) show the fitted and projected mortality rates. The fan charts are based on 10 000 simulations. On top of that, we add the mortality rate projections of the earlier discussed mortality model in blue, i.e. the mortality model that uses a calibration period 1988-2019 and an AR(1) process to model κ_t. Apart from the plot showing the projection of a 25-year old male, we do not observe many differences.

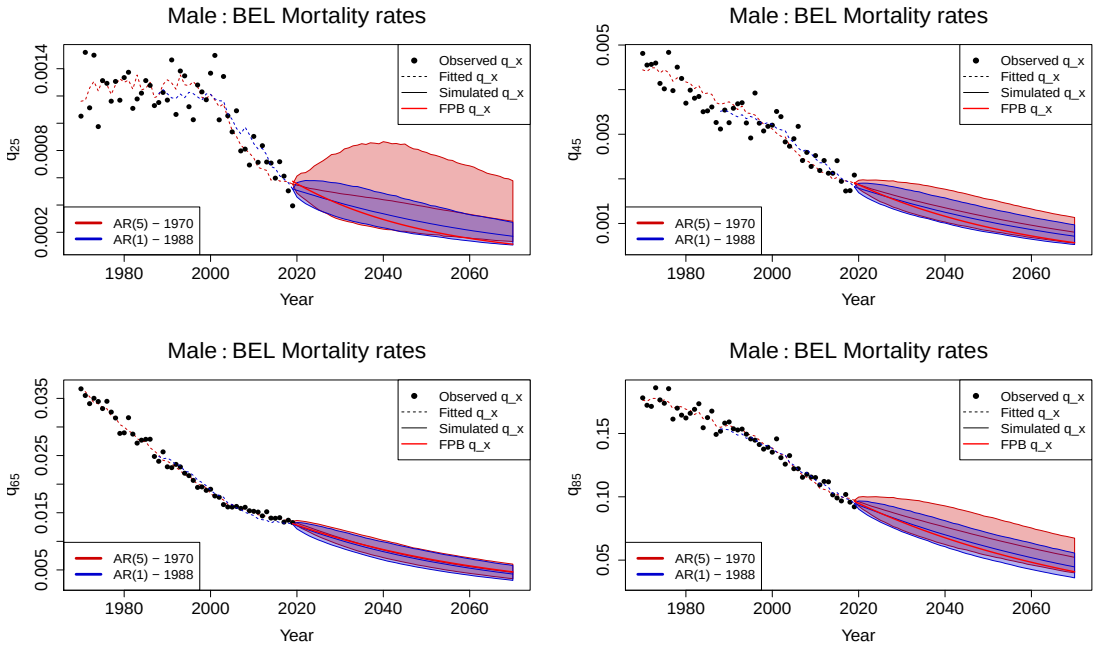

Figure 25: Estimated and projected mortality rates, $q_{x,t}$, for Belgium, male data, ages 25, 45 (top row) and 65, 85 (bottom row). We plot 0.5% quantile, median and 99.5% quantile obtained from 10 000 simulations. We add the mortality rate projections of Figure 9 in blue.

C.3 Life expectancy: period and cohort

The top panels of Figure 27 show the observed period life expectancy (black dots) for a 0 (left) and 65 (right) year old male, the calibrated period life expectancy (red line) and the simulations of $e_0(t)$ and $e_{65}(t)$ for $t = 2020, \ldots, 2070$, as obtained with the AR(5) model for κ_t^M. The blue fan chart shows the cohort life expectancy, $e_0^{\text{coh}}(t)$ and $e_{65}^{\text{coh}}(t)$. The corresponding results for females are in the bottom panels of Figure 27. We add in purple the period and cohort life expectancies resulting from the mortality model with the shorter calibration period starting in the year 1988 (see Figure 11).

Table 6 lists the median and 99% confidence intervals of $e_x^{\text{coh}}(t)$ for some specific choices of x and t. We add the results of Table 2 to make a comparison between the two approaches. The mortality model that uses the AR(5) time series to model κ_t^M and the AR(1) model for κ_t^F (longer calibration period) underestimates the cohort life expectancies compared to the mortality model that uses the AR(1) time series model to model both κ_t^M and κ_t^F (shorter calibration period), in the case of males. In the case of females, we have an overestimation.

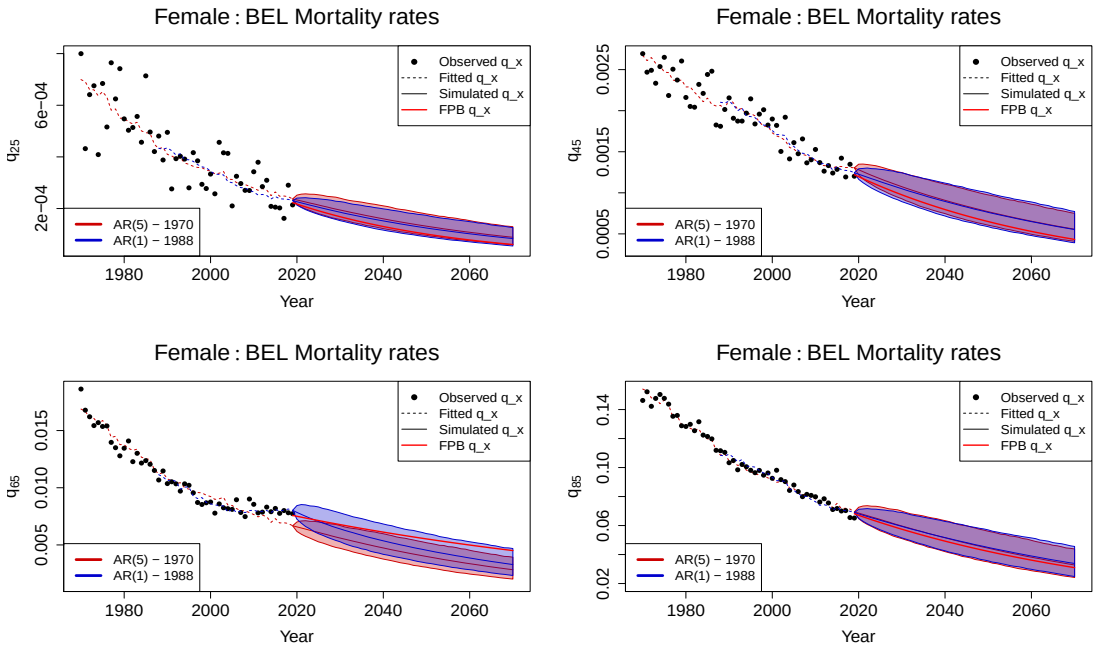

Figure 26: Estimated and projected mortality rates, $q_{x,t}$, for Belgium, female data, ages 25, 45 (top row) and 65, 85 (bottom row). We plot 0.5% quantile, median and 99.5% quantile obtained from 10 000 simulations. We add the mortality rate projections of Figure 10 in blue.

year		males		females	
		0	65	0	65
2020	$[q_{0.5};q_{50};q_{99.5}]_{\text{AR}(5)}$	[86.91;88.81;90.43]	[18.98;19.91;20.83]	[90.18;92.14;93.78]	[22.30;23.33;24.33]
	$[q_{0.5};q_{50};q_{99.5}]_{\text{AR}(1)}$	[88.11;89.89;91.46]	[19.57;20.37;21.17]	[89.46;91.53;93.25]	[22.15;23.14;24.07]
	FPB	(90.07;90.25)	(20.11;20.56)	(91.28;91.53)	(22.92;23.38)
2040	$[q_{0.5};q_{50};q_{99.5}]_{\text{AR}(5)}$	[89.15;90.93;92.46]	[20.85;22.21;23.49]	[91.93;93.83;95.41]	[23.77;25.30;26.67]
	$[q_{0.5};q_{50};q_{99.5}]_{\text{AR}(1)}$	[90.35;92.08;93.52]	[21.65;22.94;24.14]	[91.12;93.14;94.82]	[23.63;25.09;26.46]
	FPB	(92.09;92.36)	(22.79;23.26)	(92.80;93.08)	(24.82;25.28)
2060	$[q_{0.5};q_{50};q_{99.5}]_{\text{AR}(5)}$	[90.97;92.56;93.95]	[22.70;24.21;25.58]	[93.44;95.16;96.60]	[25.32;27.02;28.47]
	$[q_{0.5};q_{50};q_{99.5}]_{\text{AR}(1)}$	[92.18;93.72;94.97]	[23.69;25.11;26.39]	[92.50;94.45;95.97]	[25.06;26.74;28.18]
	FPB	(93.62;93.90)	(25.00;25.48)	(94.06;94.34)	(26.45;26.92)

Table 6: Cohort life expectancy for a 0 and 65 year old, 0.5% quantile, median and 99.5% quantile obtained from 10 000 simulations, males and females. 'FPB' refers to Federaal Planbureau (2020); the first number is the cohort life expectancy as published in Federaal Planbureau (2020) (i.e. using *ages in completed years*) and the second number is the cohort life expectancy at exact ages, using Jaumain and Vandeschrick (2012). The subscript AR(5) refers to the mortality model discussed in this section, the subscript AR(1) refers to the mortality model with calibration period 1988-2019 and where we used an AR(1) process to model both κ_t^M and κ_t^F.

D Bootstrapping

In line with Koninklijk Actuarieel Genootschap (2018), we now investigate the uncertainty of the parameter estimates $\hat{A}_x, \hat{B}_x, \hat{K}_t, \hat{\alpha}_x, \hat{\beta}_x$ and $\hat{\kappa}_t$ in the LL model on the one hand and the

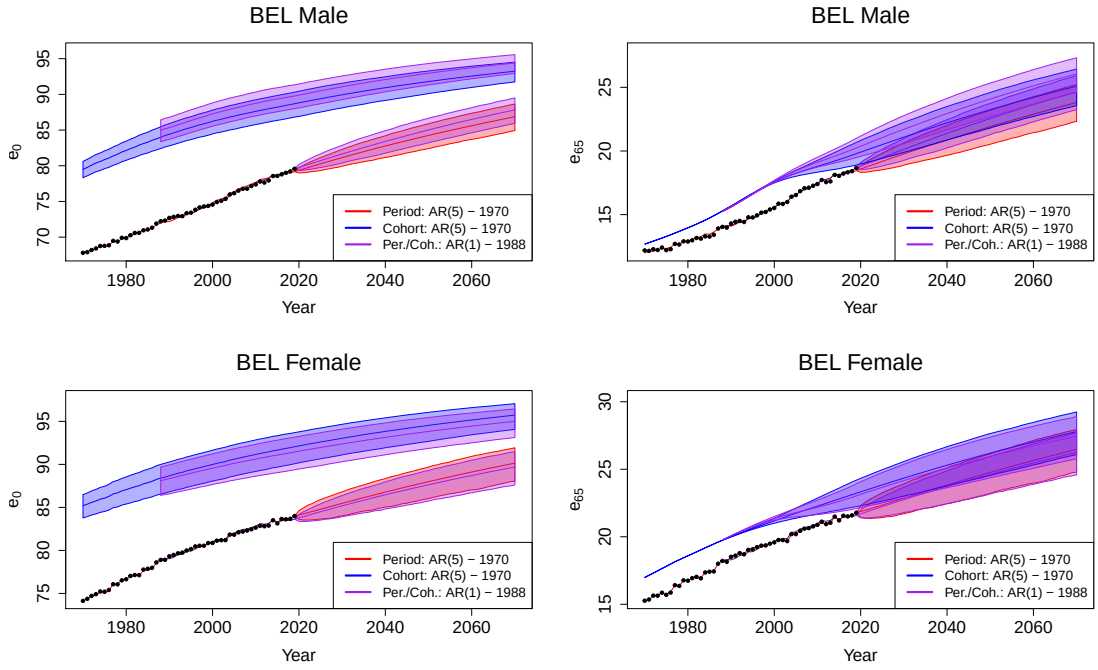

Figure 27: Period (black dots and red lines) and cohort (blue) life expectancy for a 0 year old (left) and 65 year old (right), male (top) and female (bottom) data. We plot 0.5% quantile, median and 99.5% quantile obtained from 10 000 simulations. We add the results of Figure 11 in purple.

parameters used in the time series dynamics on the other hand. We cannot analytically derive the prediction intervals of these parameter estimates. Therefore, we rely on bootstrapping to assess the parameter uncertainty.

We again model the Belgian period effect κ_t using an AR(1) process instead of the more complex AR(5) process, covered in Appendix C. We use the calibration periods 1988-2018 (European trend) and 1988-2019 (Belgian deviation) in our experiments. Our goal is to investigate the uncertainty of the parameter estimates. However, the choice of the calibration periods does not ensure stability for the time series of the estimated Belgian period effect $\hat{\kappa}_t$ in each of the bootstrapped data sets.

We will asses the uncertainty using the Poisson bootstrap approach, as discussed in Pitacco et al. (2009). We adjust their proposed strategy since we work with the LL model, combining a mortality model for the European trend with a model for the Belgian deviation from this trend.

1. We start with the observations $(E_{x,t}^{\text{BEL}}, d_{x,t}^{\text{BEL}})$, representing the exposures and number of deaths in Belgium at ages x and times t. Then, we take B bootstrap samples $(E_{x,t}^{\text{BEL}}, d_{x,t}^{\text{BEL},b})$ for $b = 1, 2, \ldots, B$. The bootstrapped number of deaths $d_{x,t}^{\text{BEL},b}$ are realizations of the Poisson distribution with mean $E_{x,t}^{\text{BEL}} \hat{\mu}_{x,t}^{\text{BEL}} = \hat{d}_{x,t}^{\text{BEL}}$, where the $\hat{\mu}_{x,t}^{\text{BEL}}$'s are the fitted mortality rates for Belgium and are calculated using Equations (2), (3) and (4) based on the calibrated mortality model. In other words, we add different Poisson noises to the calibrated number of deaths $\hat{d}_{x,t}^{\text{BEL}}$ to end up with the bootstrapped number of deaths $d_{x,t}^{\text{BEL},b}$.

2. Besides the Belgian exposures and number of deaths, we also work with West-European

data $(E^{\text{EU}}_{x,t}, d^{\text{EU}}_{x,t})$ to model the European mortality trend. We again take B bootstrap samples $(E^{EU}_{x,t}, d^{\text{EU},b}_{x,t})$, where now the bootstrapped number of deaths of the European countries $d^{EU,b}_{x,t}$ are drawn from a Poisson distribution with mean $E^{\text{EU}}_{x,t}\hat{\mu}^{\text{EU}}_{x,t} = \hat{d}^{\text{EU}}_{x,t}$. We hereby calculate the fitted mortality rates of European $\hat{\mu}^{\text{EU}}_{x,t}$'s using Equation (3), based on the estimated $\hat{A}_x, \hat{B}_x$ and $\hat{K}_t$.

To conclude, we have B bootstrap samples of the Belgian and total West-European data, namely $(E^{\text{BEL}}_{x,t}, d^{\text{BEL},b}_{x,t})$ and $(E^{\text{EU}}_{x,t}, d^{\text{EU},b}_{x,t})$ for $b = 1, 2, \ldots, B$. For each b, we then repeat the calibration process documented in Section 2.4. This then leads to B parameter estimates of the common trend, $\hat{A}^b_x, \hat{B}^b_x$ and $\hat{K}^b_t$, and for the Belgian deviation of this trend, $\hat{\alpha}^b_x, \hat{\beta}^b_x$ and $\hat{\kappa}^b_t$.

Figure 28 shows the 99% bootstrap confidence intervals of the estimates of the European parameters, namely $\hat{A}^b_x, \hat{B}^b_x$ and $\hat{K}^b_t$ for females, calculated on each bootstrap sample. Figure 29 shows the results for the estimated Belgian female parameters $\hat{\alpha}^b_x, \hat{\beta}^b_x$ and $\hat{\kappa}^b_t$. We use $B = 10\,000$ bootstrap samples. Figure 30 and 31 show the corresponding figures for males.

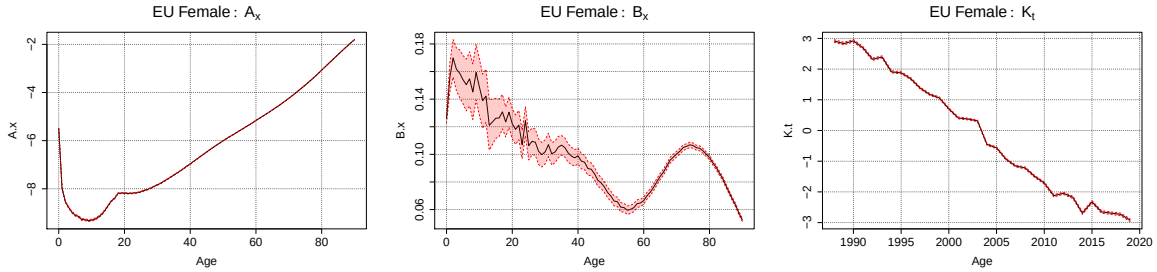

Figure 28: Estimated common parameters, female data, ages 0-90, years 1988-2018: $\hat{A}^b_x$, $\hat{B}^b_x$ and $\hat{K}^b_t$ for each bootstrap sample $b = 1, 2, \ldots, B$. We add the 99% bootstrap confidence intervals in red. The black line represents the medium quantile.

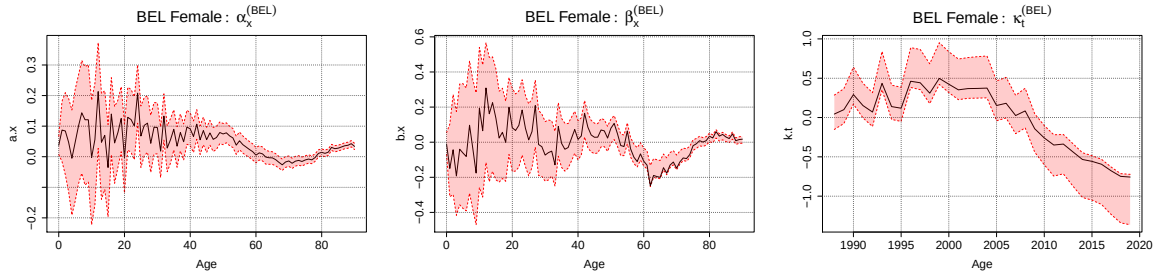

Figure 29: Estimated parameters for Belgium, female data, ages 0-90, years 1988-2019: $\hat{\alpha}^b_x$, $\hat{\beta}^b_x$ and $\hat{\kappa}^b_t$ for each bootstrap sample $b = 1, 2, \ldots, B$. We add the 99% bootstrap confidence intervals in red. The black line represents the medium quantile.

In addition, Figure 32 shows the 99% bootstrap confidence intervals of the estimated male, Belgian mortality rates $\hat{q}^b_{x,t}$ for ages 25, 45, 65 and 85. These mortality rates are calculated as follows:

$$\hat{\mu}^{\text{BEL},b}_{x,t} = \exp\left(\hat{A}^b_x + \hat{\alpha}^b_x + \hat{B}^b_x\hat{K}^b_t + \hat{\beta}^b_x\hat{\kappa}^b_t\right)$$
$$\hat{q}^{\text{BEL},b}_{x,t} = 1 - \exp\left(-\hat{\mu}^{\text{BEL},b}_{x,t}\right),$$

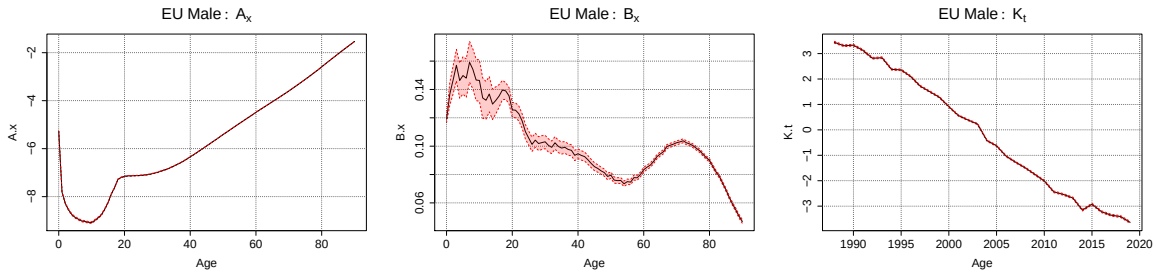

Figure 30: Estimated common parameters, male data, ages 0-90, years 1988-2018: $\hat{A}_x^b$, $\hat{B}_x^b$ and $\hat{K}_t^b$ for each bootstrap sample $b = 1, 2, \ldots, B$. We add the 99% bootstrap confidence intervals in red. The black line represents the medium quantile.

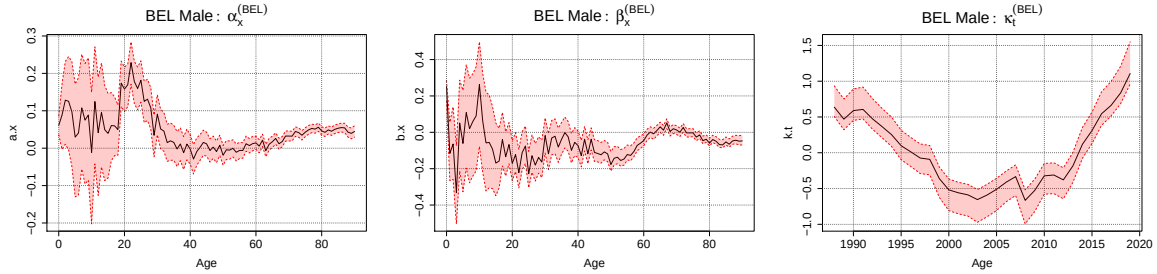

Figure 31: Estimated parameters for Belgium, male data, ages 0-90, years 1988-2019: $\hat{\alpha}_x^b$, $\hat{\beta}_x^b$ and $\hat{\kappa}_t^b$ for each bootstrap sample $b = 1, 2, \ldots, B$. We add the 99% bootstrap confidence intervals in red. The black line represents the medium quantile.

for $x \in \{25,\ 45,\ 65,\ 85\}$, $t \in \{1988,\ 1989, \ldots, 2019\}$, and $b \in \{1, 2, ..., 10\ 000\}$. The black line shows the estimated Belgian mortality rates of the original LL fit, on the original (non-bootstrapped) data set. The black dots are the observed mortality rates. Figure 33 shows the same results for females.

Next, we can repeat the projection procedure, covered in Section 2.5, for each bootstrap sample. We choose an AR(1) process to model the Belgian period effect $\hat{\kappa}_t^b$. More specifically, we again follow the time dynamics in Equations (5) and (6) and use the 10 000 bootstrap samples for the time dependent parameters. Figure 34 shows the histogram of the bootstrap estimates of the drift parameter in the random walk process to model the European period effect $\hat{K}_t^M$ and $\hat{K}_t^F$. Further, a stable mortality model requires that the estimated AR-paremeter is smaller than 1 in absolute value. The bottom panels in Figure 35 show histograms of the bootstrap estimates of the AR-parameter for both males and females. Figure 35 shows the histograms of the intercepts in the AR(1) process for $\hat{\kappa}_t^M$ and $\hat{\kappa}_t^F$ at the top panels. Lastly, histograms of the parameter estimates in the covariance matrix $\hat{C}$ as a result of the bootstrapping are given in Figure 36.

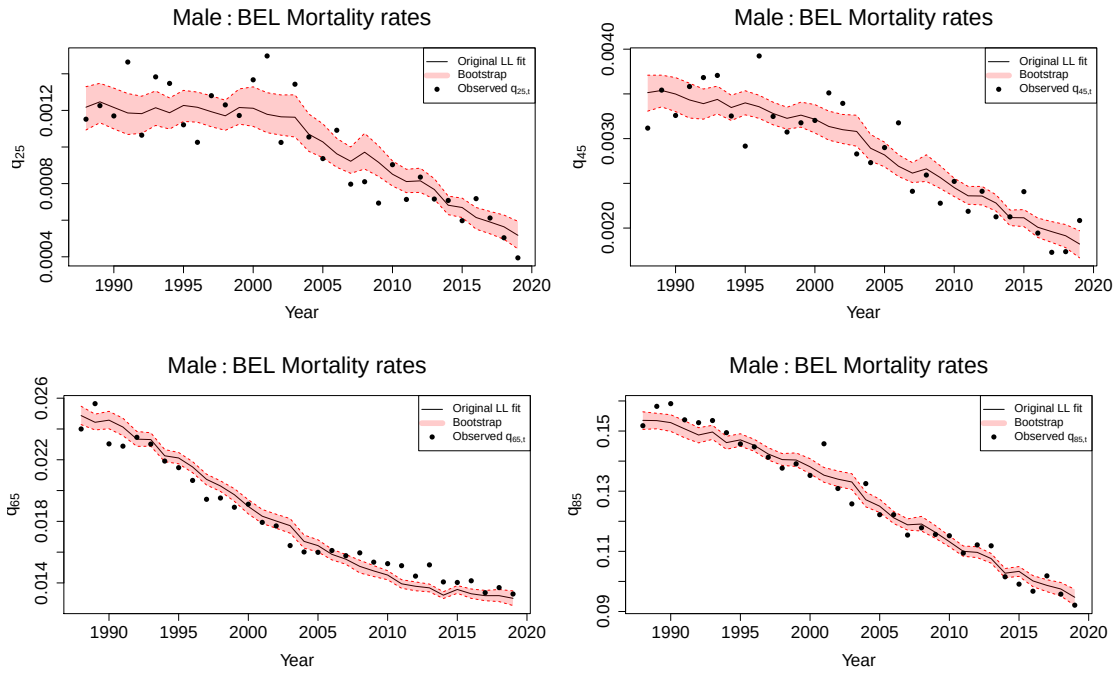

Figure 32: Fitted mortality rates $\hat{q}_{x,t}$, for Belgium, male data, ages 25, 45 (top row) and 65, 85 (bottom row), calibration period $1988-2019$. We add the 99% bootstrap confidence intervals for $\hat{q}_{x,t}$ in red. The black line represents the fitted mortality rates, based on the original LL fit (on the original data set).

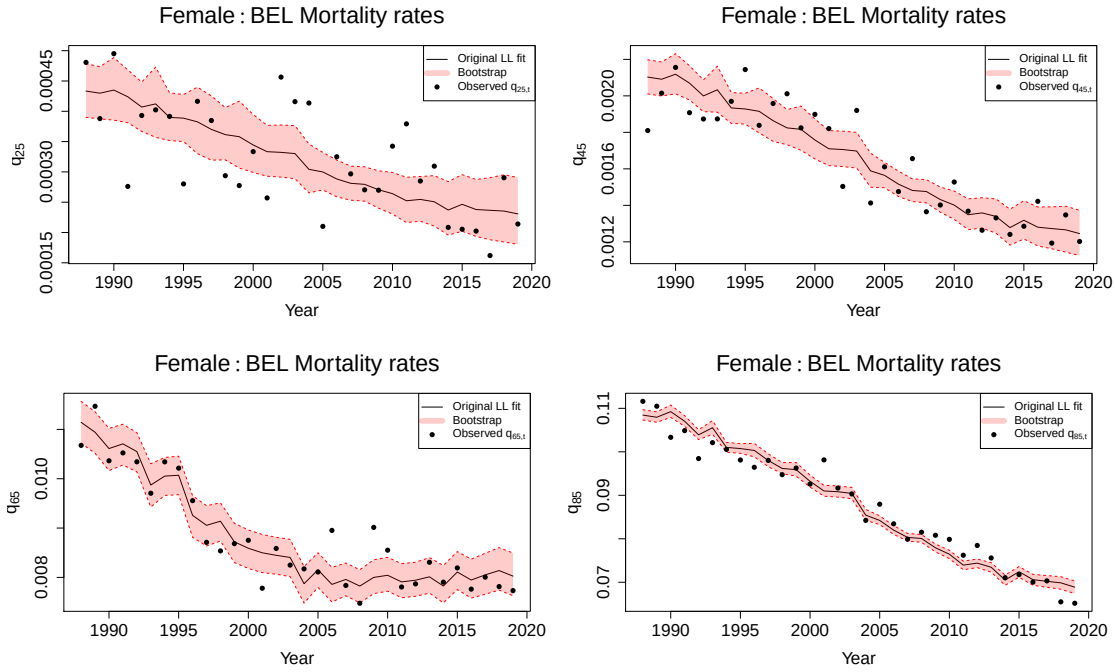

Figure 33: Fitted mortality rates $\hat{q}_{x,t}$, for Belgium, female data, ages 25, 45 (top row) and 65, 85 (bottom row), calibration period $1988-2019$. We add the 99% bootstrap confidence intervals for $\hat{q}_{x,t}$ in red. The black line represents the fitted mortality rates, based on the original LL fit (on the original data set).

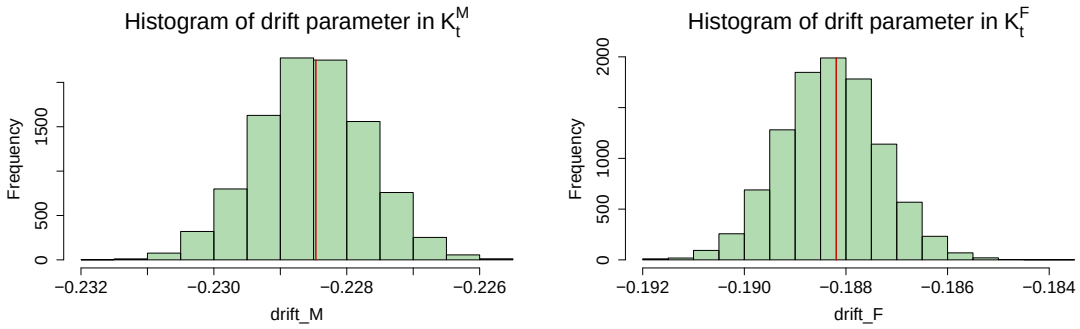

Figure 34: Histogram of the bootstrapped estimates of the drift parameter in the random walk process to model the European period effect $\hat{K}_t^M$ for males (left) and $\hat{K}_t^F$ for females (right). The vertical, green, solid line shows the original estimate of the drift parameter (see Table 1). The mortality model is calibrated on male and female data for years 1988-2018 (European trend) and 1988-2019 (Belgian deviation), and ages 0-90.

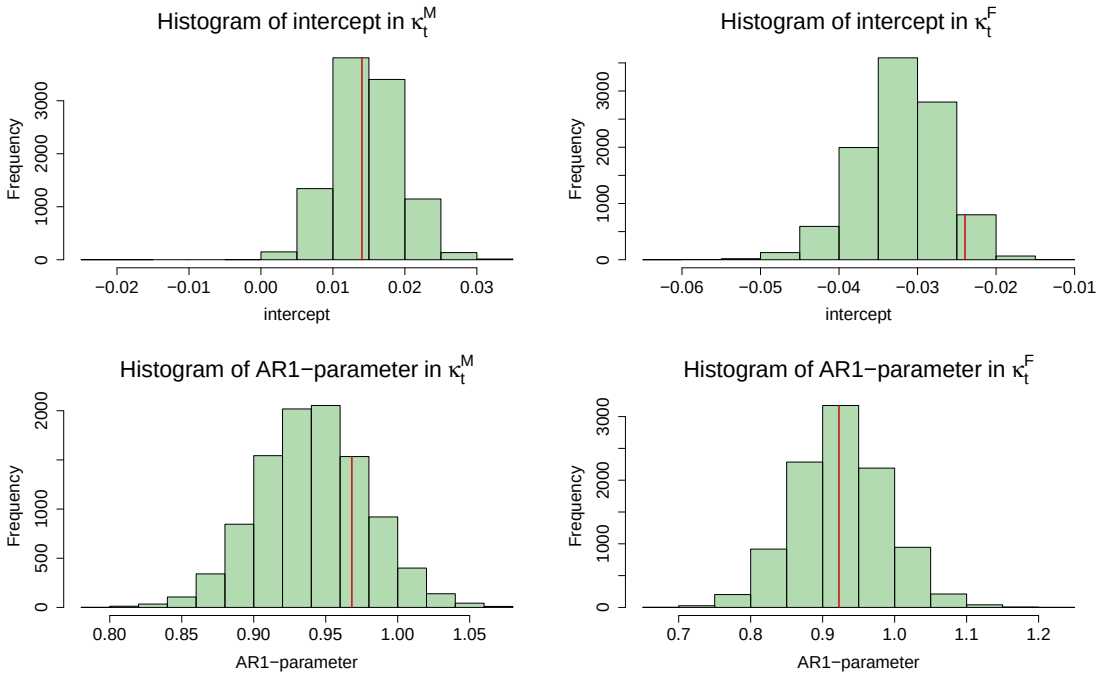

Figure 35: Histogram of the bootstrapped estimates of the intercept (top) and the AR(1) parameter (bottom) in the time series process to model the Belgian period effect $\hat{\kappa}_t$ for males (left) and females (right). The vertical, red, solid line shows the original parameter estimates (see Table 1). The mortality model is calibrated on male and female data for years 1988-2018 (European trend) and 1988-2019 (Belgian deviation), and ages 0-90.

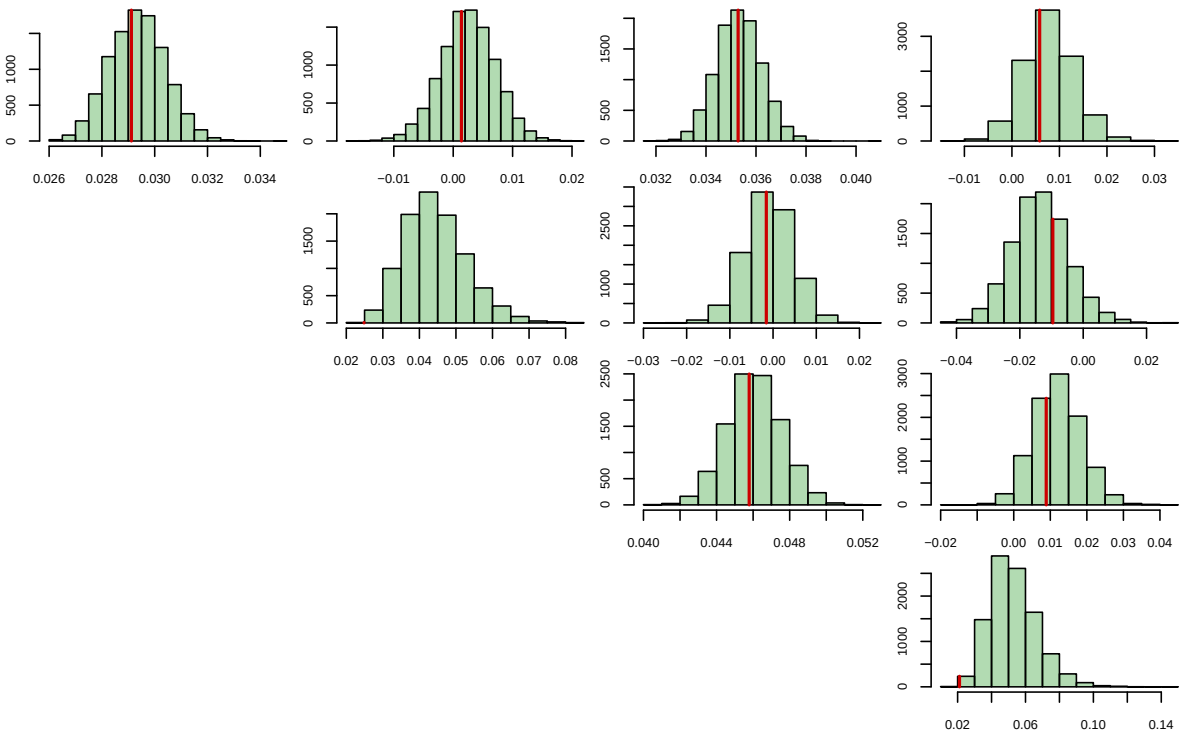

Figure 36: Histograms of the parameter estimates in the covariance matrix $\hat{C}$ for the error terms $\left(\varepsilon_t^M, \delta_t^M, \varepsilon_t^F, \delta_t^F\right)$ in the multivariate time series processes we used for $(\hat{K}_t^M, \hat{\kappa}_t^M, \hat{K}_t^F, \hat{\kappa}_t^F)$. The vertical, red, solid line shows the original parameter estimates (see Table 1). Mortality model is calibrated on male and female data for years 1988-2018 (European trend) and 1988-2019 (Belgian deviation), and ages 0-90.